Magnetic Implants *In Vivo* Guiding Sorafenib Liver Delivery By Superparamagnetic Solid Lipid Nanoparticles

Rosa Maria Iacobazzi[a,#], Fabio Vischio[b,c,#], Ilaria Arduino[d], Fabio Canepa[e], Valentino Laquintana[d], Maria Notarnicola[f], Maria Principia Scavo[f], Giusy Bianco[f], Elisabetta Fanizza[b,c], Angela Assunta Lopedota[d], Annalisa Cutrignelli[d], Antonio Lopalco[d], Amalia Azzariti[a], Maria Lucia Curri[b,c], Massimo Franco[d], Gianluigi Giannelli[g], Byung Chul Lee[h], Nicoletta Depalo[c,*], and Nunzio Denora[d,*]

[a] IRCCS Istituto Tumori "Giovanni Paolo II", Via O. Flacco 65, 70124 Bari, Italy (r.m.iacobazzi@oncologico.bari.it; a.azzariti@oncologico.bari.it)

[b] Department of Chemistry, University of Bari, Via E. Orabona 4, 70125 Bari, Italy (fabio.vischio@uniba.it; elisabetta.fanizza@uniba.it; marialucia.curri@uniba.it)

[c] CNR-Institute for Chemical-Physical Processes (IPCF) Bari Division, Via Orabona 4, 70125 Bari, Italy (n.depalo@ba.ipcf.cnr.it)

[d] Department of Pharmacy - Pharmaceutical Sciences, University of Bari, Via E. Orabona 4, 70125 Bari, Italy (ilaria.arduino@uniba.it; valentino.laquintana@uniba.it; angelaassunta.lopedota@uniba.it; annalisa.cutrignelli@uniba.it; antonio.lopalco@uniba.it; massimo.franco@uniba.it; nunzio.denora@uniba.it)

[e] Department of Chemistry and Industrial Chemistry, University of Genoa, 16146 Genoa, Italy (Fabio.Canepa@unige.it).

[f] National Institute of Gastroenterology "S. de Bellis," Personalized Medicine Laboratory, Via Turi 26 Castellana Grotte, Bari, Italy (maria.notarnicola@irccsdebellis.it; maria.scavo@irccsdebellis.it; giusi.bianco@irccsdebellis.it)

[g] Scientific Direction, National Institute of Gastroenterology "de Bellis," Via Turi 26 Castellana Grotte, Bari, Italy (gianluigi.giannelli@irccsdebellis.it)

[h] Department of Nuclear Medicine, Seoul National University College of Medicine, Seoul National University Bundang Hospital, Seongnam 13620, Republic of Korea (leebc@snu.ac.kr)

[#] The authors R. M. Iacobazzi and F. Vischio contributed equally to this work.

*Corresponding Authors: Dr. N. Depalo, (n.depalo@ba.ipcf.cnr.it, CNR-IPCF Bari Division, c/o, Department of Chemistry, University of Bari, Via Orabona, 4, 70126 Bari, Italy, phone number: +39 080 5442027), Prof. N. Denora (nunzio.denora@uniba.it, Department of Pharmacy - Pharmaceutical Sciences, University of Bari, Via E. Orabona 4, 70125 Bari, Italy, phone number: +39 0805442767)

Abstract

Hypothesis
Solid lipid nanoparticles (SLNs), co-encapsulating superparamagnetic iron oxide nanoparticles and sorafenib, have been exploited for magnetic-guided drug delivery to the liver. Two different magnetic configurations, both comprising two small magnets, were under-skin implanted to investigate the effect of the magnetic field topology on the magnetic SLNP accumulation in liver tissues. A preliminary simulation analysis was performed to predict the magnetic field topography for each tested configuration.

Experiments
SLNs were prepared using a hot homogenization approach and characterized using complementary techniques. Their *in vitro* biological behavior was assessed in HepG-2 liver cancer cells; wild-type mice were used for the *in vivo* study. The magnet configuration that resulted in a higher magnetic targeting efficiency was investigated by evaluating the iron content in homogenated murine liver tissues.

Findings
SLNs, characterized by an average size smaller than 200 nm, retained their superparamagnetic behavior and relevant molecular resonance imaging properties as negative contrast agents. The evaluation of iron accumulation in the liver tissues was consistent with the magnetic induction profile of each magnet configuration, concurring with the results predicted by simulation analysis and obtained by measurements in living mice.

Keywords
Solid Lipid Nanoparticles, Sorafenib, SPIONs, Liver Magnetic Targeting, HepG-2 Cancer Cells, Magnetic Field Topography

ABBREVIATIONS

BSA, bovine serum albumin; CP, cetyl palmitate; DC, quasi-static magnetization; D_H, average hydrodynamic diameter; DL, drug loading; DLS, dynamic light scattering; DMSO, dimethyl sulfoxide; EE, encapsulation efficiency; FEMM, finite element method magnetics; FOV, field of view; HCC, hepatocellular carcinoma; HPLC, high-performance liquid chromatography; ICP-

AES, inductively coupled plasma atomic emission spectrometry; ICP-MS, inductively coupled plasma mass spectrometry; ICP-OES, inductively coupled plasma emission spectroscopy instrument; MEMS, multi-echo multiple slice; MRI, magnetic resonance imaging; MTT, 3-(4,5-dimethylthiazol-2-yl)-2,5-diphenyltetrazolium bromide; NdFeB, neodymium magnets; NPs, nanoparticles; PBS, phosphate-buffered saline; PDI, polydispersity index; PEG-2-PE, 1,2-dipalmitoyl-sn-glycero-3-phosphoethanolamine-N-[methoxy(polyethyleneglycol)-2000] (ammonium salt); RT, room temperature; SLNs, solid lipid nanoparticles; SPIONs, superparamagnetic iron oxide nanoparticles; T2, transverse relaxation time; TE, echo time; TEM, transmission electron microscopy; TR, repetition time.

1. INTRODUCTION

Hepatocellular carcinoma (HCC) is the most common cause of liver cancer, with a globally increasing incidence. Unfortunately, no effective treatment is available for patients with advanced stages of HCC [1, 2]. Among the standard treatments for HCC, including surgery, liver transplantation, and chemotherapy, also combined with chemoembolization and thermoablation, chemotherapy presents limitations because, although most drugs reach high liver concentrations, they are rapidly cleared and metabolized. Numerous biological studies have been performed to identify the biochemical pathways underlying HCC progression and, ultimately, to identify an effective therapy with reduced side effects [3].

Sorafenib, a tyrosine kinase inhibitor, is one of the most commonly used first-line chemotherapeutic agents for HCC, as it has been found to prolong patient survival [2, 4, 5]; however, the occurrence of severe side effects and pharmaco-resistance may require interruption of the treatment [6–8]. Furthermore, the limited solubility of sorafenib in aqueous environments strongly limits its application in local treatments.

In vitro cellular and preclinical studies have proven the high permeability of sorafenib across gastrointestinal epithelia, thus possibly enabling its classification as a class II drug in the Biopharmaceutics Classification System approved by the Food and Drug Administration [9,10]. Currently, oral administration of sorafenib using tablets is not considered the most suitable dosage form, owing to its poor water solubility. The combination of sorafenib and transarterial chemoembolization represents an adjunctive treatment to the use of sorafenib alone, providing a significant overall survival benefit for patients. However, such a combined therapeutic approach is applicable only to patients with satisfactory liver functional reserve [11–15]. Consequently, there is a high demand for new, reliable, and increasingly efficient formulations [16].

A critical issue to tackle in HCC therapy is the preferential accumulation of the therapeutic agent and the ability to increase its residence time in liver tissue [17, 18]. To guide nanoparticles (NPs) to the target, the most common strategy in different types of cancer relies on their surface functionalization with specific targeting units such as antibodies, nanobodies, small molecules, toxins, and receptor-specific molecules [19, 20]. A valuable and alternative approach for site-directed drug targeting relies on magnetic NP-driven delivery systems, as magnetic fields may act at relatively long distances without damaging biological tissues [21, 22]. The most common approach for magnetic targeting is based on the application of a magnetic field generated using external permanent magnets to drive and concentrate the NPs at the target sites. The magnet geometry and tumor-to-magnet distance were found to be essential parameters for controlling the effectiveness of magnetic drug delivery for clinical purposes [23]. Recently, the use of a two-magnet configuration was suggested as a successful strategy to achieve advanced external magnetic targeting, as it enhanced magnetic NP accumulation in solid tumors at a distance > 5 mm from the magnet surface [24, 25]. Furthermore, magnetic or magnetizable implants can be placed

by surgical intervention, generally in the lumen of a blood vessel, as an alternative and effective strategy to enhance the magnetic field and overcome limitations in using magnetic targeting in superficial tumors [22, 26]. In particular, for liver magnetic targeting, external magnets have mostly been tested *in vivo* [27–30], whereas very few studies have reported on *in vivo* magnetic implant-assisted targeting [31].

The aim of this study was to fabricate polyethylene glycol (PEG)-modified solid lipid NPs (SLNs) loaded with both organic capped superparamagnetic iron oxide NPs (SPIONs) and sorafenib and to investigate their ability to accumulate in the liver as efficient drug delivery nanocarriers driven by designed magnetic implants. SLNs are physiological lipid-based colloidal nanocarriers and, compared with the traditional colloidal carriers such as polymeric NPs and liposomes, are efficient in protecting the drug from degradation and metabolic inactivation, enhancing the bioavailability of poorly water-soluble drugs and ensuring controlled drug release [32]. SLNs were also found to be suitable for encapsulating robust inorganic NPs such as SPIONs and luminescent or plasmonic colloidal nanocrystals [33–35]. Numerous and diverse types of nanocarriers have been investigated to improve the bioavailability, efficacy, and safety profile of sorafenib for the therapy of HCC [20,36–43]. By contrast, only a few studies have described the use of magnetic NPs as sorafenib delivery vehicles [33, 44–47]. Among magnetic NPs, biodegradable SPIONs are attractive for magnetically driven targeting, as no remnant magnetization occurs in the absence of an applied field, owing to their superparamagnetic state; consequently, their aggregation in biological fluids is avoided, and they can be precisely remotely controlled. Furthermore, as SPIONs act as efficient contrast agents in conventional magnetic resonance imaging (MRI), they can offer benefits derived from simultaneous magnetic targeting and tumor imaging [48–50].

Sorafenib-loaded superparamagnetic SLNs were extensively characterized in their morphological and magnetic properties, colloidal stability, encapsulation efficiency, and drug loading. Their imaging properties as MRI contrast agents were also investigated by performing *in vitro* phantom tests, and the effect of the magnetic field on their antitumor efficacy was evaluated in an *in vitro* study performed on HepG-2 liver cancer cells. An *in vitro* flow system was designed and used to investigate the ability of the superparamagnetic SLNs to be held back when exposed to a magnetic field generated by two micromagnets under simulated liver blood flow circulation. Furthermore, preliminary 2D-magnetic-field maps, resulting from two different small magnet configurations, were obtained using a simulation analysis to predict their corresponding magnetic field gradient and topography and thus optimize the experimental conditions for the *in vivo* magnetic targeting study. Finally, under-skin micromagnets were implanted *in vivo*, above the liver of living wild-type mice, through a minimally invasive surgical intervention, and the two different magnet configurations of the magnets were exploited to assess the effect of their magnetic field topographies on the accumulation in the target organ.

2. Materials and methods

2.1. Materials

All solvents, polysorbate 80 (Tween 80), phosphotungstic acid (99.995%), molybdenum blue spray reagent, and dimethylthiazol-diphenyltetrazolium bromide (MTT), were purchased from Sigma-Aldrich. Additionally, 1,2-dipalmitoyl-sn-glycero-3-phosphoethanolamine-N-[methoxy(polyethyleneglycol)-2000] (ammonium salt) (PEG-2-PE) was obtained from Avanti Polar Lipids. Cetyl palmitate (CP) was purchased from Farmalabor (Canosa di Puglia, Italy). Sorafenib tosylate was acquired from Selleck Chemicals LLC, while Bradford reagent was purchased from Bio-Rad. A Milli-Q gradient A-10 system (Millipore, 18.2 MΩcm, organic carbon

content ≥ 4 μg/L) was used to obtain ultrapure water to prepare the aqueous solutions. All materials used for cell culture were purchased from EuroClone, Italy. Disposable culture flasks and Petri dishes were obtained from Corning (Corning, NY, USA).

2.2. Preparation of SLNs loaded with SPIONs and sorafenib

SPIONs were synthesized and purified according to a previously reported experimental procedure [47, 51]. Finally, they were dispersed in chloroform to obtain a clear, stable colloidal solution at a final concentration of 12.7 mg/mL.

PEG-SLNs loaded with sorafenib and SPIONs (Sorafenib/SPIONs/PEG-SLNs), were prepared using an oil-in-water homogenization process at a high temperature, according to experimental procedures previously reported in the literature, with some modifications [33, 34, 52].

CP (200 mg), PEG-2-PE (4% w/w, with respect to the CP weight), and calibrated amounts of the SPION stock dispersion were dissolved in chloroform (1 mL) at 60 °C. Sorafenib was solubilized in methanol (500 μL) at 65 °C for 60 min under vigorous stirring; the resulting solution was mixed with the lipid mixture to form the organic phase. Tween 80 (180 mg) was dissolved in pure water (3 mL) to obtain the aqueous phase at a final concentration of 45 mM. The organic solution was gently mixed with the aqueous solution at 60 °C and then sonicated for 5 min (Branson Sonifier 150). The resulting oil-in-water emulsion was transferred into a round-bottom flask, and the organic solvent was rapidly evaporated under reduced pressure at 60 °C using a rotary evaporator (Buchi, Switzerland). Centrifugation (5000 ×g for 1 min) was carried out to remove any excess of SPIONs, possibly not embedded in the lipid core of Sorafenib/SPIONs/PEG-SLNs. Finally, Sorafenib/SPIONs/PEG-SLNs were further purified using Centriplus YM100 (Millipore, Bedford, MA, USA) with water (Mw cutoff =100 kDa) and then stored at 4 °C. According to the same

experimental procedure, bare and empty SLNs were prepared using the same lipid mixture without the addition of PEG-2-PE, SPIONs, or sorafenib, while SLNs were loaded only with SPIONs (SPIONs/PEG-SLNs) without the addition of sorafenib.

2.3. Determination of the amount of sorafenib and SPIONs encapsulated in SLNs

The amount of sorafenib entrapped in Sorafenib/SPIONs/PEG-SLNs is expressed as drug loading (DL%) and encapsulation efficiency (EE%) [20]. It was determined by dissolving SLNs in hexane, solubilizing the lipid matrix, and extracting the drug with dimethyl sulfoxide. An Agilent 1260 Infinity Quaternary LC System equipped with an ultraviolet (UV)-visible 1260 Infinity Multiple Wavelength Detector and Rheodyne Manual Sample Injector Valves 7725i was employed for high-performance liquid chromatography-UV (HPLC-UV) analysis. Sorafenib was separated on a Zorbax Eclipse Plus C18 column (4.6×250 mm, 5 mm). The mobile phase consisted of a mixture of Milli-Q water and methanol (at a ratio of 20:80 v/v) and was pumped at a flow rate of 1 mL/min at 25 °C. The UV detector was set at 250 nm. A calibration curve of pure sorafenib was obtained in the range of 0–1 g/L.

2.4. In vitro drug release

The drug release was investigated by introducing 500 µL of Sorafenib/SPIONs/PEG-SLNs into a Franz cell (Cuprophan membrane, cutoff 10,000 Da, Medicell Membranes, Ltd., London) filled with phosphate-buffered saline (PBS) buffer (pH 7.4, 1% Tween 80). The cells were incubated at 37 °C in a thermostatic bath for 24 h. At fixed time points, 300 µL of the solution was removed for HPLC analysis and replaced with fresh buffer solution. HPLC analysis was performed as described in section 2.3.

2.5. Particle size, size distribution, and colloidal stability

A Zetasizer Nano ZS (Malvern Instruments Ltd., Worcestershire, UK [DTS 5.00]) was used to perform dynamic light scattering (DLS) analysis and ζ-measurements on SLN samples, according to previously published procedures [47]. The ζ-measurements were performed in a PBS buffer solution (10 mM) at pH 7.4. All reported data are presented as mean values ± standard deviation of three replicates.

2.6. Transmission electron microscopy analysis

A Jeol JEM-1011 microscope was employed for the transmission electron microscopy (TEM) investigation working at an accelerating voltage of 100 kV and equipped with an Olympus Quemesa Camera (11 Mpx). Five microliters of SPIONs dispersed in chloroform or SLNs dispersed in ultrapure water were deposited on a TEM grid. A freeware Image J 1.50i analysis program [https://imagej.nih.gov/ij/] was used to perform size statistical analysis of the SPION samples, thus determining their average size and size distribution. To stain of SLN samples, after solvent evaporation, the grid was carefully placed in contact with the top surface of a drop made of an aqueous phosphotungstic acid solution of 2% (w/v) for 15 or 60 s. Finally, the grid was carefully washed and dried before the TEM micrographs were recorded.

2.7. Magnetic investigation

2.7.1. Magnetic characterization

Room-temperature (RT) direct current (DC) magnetization measurements were carried out in a -50-50 kOe magnetic field span using a commercial DC-SQUID magnetometer (MPMS Quantum Design) with a resolution higher than 10^{-8} emu (RSO option). A quantitative evaluation of the SPIONs in Sorafenib/SPIONs/PEG-SLNs was achieved by comparing the RT magnetic hysteresis cycles performed on the Sorafenib/SPIONs/PEG-SLNs and bare SPIONs.

2.7.2. MR phantom test

The Fe concentration in the Sorafenib/SPIONs/PEG-SLNs formulations was determined using Optima 530 DV, an inductively-coupled plasma emission spectroscopy instrument (Perkin Elmer). Phantom images were obtained using a 9.4 T/160 AS animal MRI system (Agilent Technologies, Santa Clara, CA, USA). The transverse relaxation time (T2) mapping was estimated using multi-echo multiple slice (MEMS) sequences with a spin-echo readout. The sequence parameters were as follows: repetition time (TR) = 3000 ms, echo time (TE) = 8.36 ms, NE = 16, average = 1, matrix size = 128×128, field of view (FOV)= 65.0×65.0 mm^2, slice thickness = 2.0 mm, and scan time = 6 min 30 s.

2.7.3. Magnetic mapping of micromagnets

The magnetic flux was measured using a high-sensitivity DSP475 Gaussmeter (Lake Shore, Inc., USA), working in the range of 1–350 kG. Magnetic flux was produced by different configurations of small permanent magnets (NdFeB N52 grade supplied by HKCM Engineering, Germany) in *in vitro* and *in vivo* experiments. Data were collected at a fixed z value, with 2 mm steps in the x- and y-directions.

2.7.4. In vitro dynamic accumulation study

The *in vitro* dynamic accumulation circuit consisted of an Erlenmeyer flask (1000 mL) as the accumulation vessel, a peristaltic pump (VELP SP311 model) working in the 1–250 mL/min flow range, a digital flowmeter (Omega Engineering FLR 1000 7D), and an accumulation system to simulate mouse livers, [30] formed by a glass cylinder (10×6 mm^2 length×internal diameter) filled with very small glass microspheres (∅ approximately 0.8 mm). Two small (2×2×3 mm^3) NdFeB permanent magnets in close contact and externally fixed to the accumulation system were used to

collect the superparamagnetic SLNs. A dispersion of Sorafenib/SPIONs/PEG-SLNs in water (98.5 mg/L) was used for the experiment, and a flow rate of 3 cm^3/min was applied to simulate the liver blood flow. The capture of the superparamagnetic SLNs was investigated by evaluating the change in Fe ion content in solution using inductively coupled plasma atomic emission spectrometry (VARIAN Vista Pro, Springvale, Australia). Data were collected every 30 min for 2 h.

2.8. In vitro study

2.8.1 Cytotoxicity assay

The human liver cancer cell line HepG-2 from Interlab Cell Line Collection (ICLC, Genova, Italy) was grown as previously reported [47]. HepG-2 cells were seeded in 96-well plates at a density of 5000 cells/well for 24 h. Subsequently, the culture medium was replaced, and the cells were incubated for 72 h with 100 µL of fresh medium containing SPIONs/PEG-SLNs, Sorafenib/SPIONs/PEG-SLNs, and sorafenib alone as a reference compound. The tested concentration range was 0–100 µM for sorafenib and 0.1–145 µg/mL for SPIONs. Cell viability was assessed using MTT assay, and results were expressed as % cell viability at each tested dose or IC_{50} values obtained using nonlinear regression in GraphPad Prism 5.0.

2.8.2. Uptake and recovery experiments

Uptake experiments were conducted following a previously described protocol [47]. After 24 h, HepG-2 cells seeded in 60 mm tissue culture dishes were further incubated for 2 and 4 h with SPIONs/PEG-SLNs (14.5 µg/mL in terms of SPIONs) with and without application of the magnetic field induced by an NdFeB ring-magnet (outer diameter of 40 mm and an inner diameter of 30 mm, B = 11.7 kG). After sample preparation, the Fe content was determined by performing ICP-MS using a Varian 820-MS ICP. The intracellular uptake of SPIONs/PEG-SLNs was

qualitatively detected after Prussian blue staining, observing the cells under an OLYMPUS CKX41 microscope [47].

The effect of magnetic targeting on the cell viability of the Sorafenib/SPIONs/PEG-SLNs was assessed on HepG-2 cells after incubation for 4 h with 10 μM of the formulations in sorafenib, both exposed or unexposed to the magnetic field, and then washed out and cultured in a fresh medium for up to 24, 48, or 72 h. Cell viability values were obtained as a percentage using the MTT assay. Sorafenib alone was used as the antitumor reference drug.

2.9. In vivo study

2.9.1 Under-skin micromagnet implantation in living wild-type mice and grouping

A total of 32 wild-type mice C57BL/6J, 9-week-old obtained from Charles River (Charles River Laboratories, Lecco, Italy) were housed and fed under specific-pathogen-free conditions according to the study protocols approved by the local ethics committee. The animal research protocol was authorized by the Italian Ministry of Health (n° 819/2017-PR, dated on the October 23, 2017). The mice were kept in temperature, air, and light-controlled conditions (lights on from 7 am to 7 pm) and received water and standard mouse food ad libitum according to the criteria outlined in the Guide for the Care and Use of Laboratory Animals [53]. All mice were housed for 1 week, and 18 received magnetic implants under general anesthesia using isoflurane inhalation (2%) (Boehringer Ingelheim Animal Health Italia S.p.A), provided by the Veterinary Unit in the Animal facility of IRCCS De Bellis of Castellana Grotte (Bari), Italy, according to the anesthesia protocols for animal management [54]. Surgery was performed to insert permanent micromagnets in two different configurations above the liver using the skin micromagnet implantation protocol. Two small NdFeB high-flux permanent magnets were used (maximum dimensions 2×2×3 mm, B = 14.3 kG).

The first configuration (A) consisted of two magnets in close contact, whereas the second configuration (B) consisted of two magnets separated by a 5 mm thick Teflon® spacer.

The mice were divided into four groups:

- Group 1: Mice with magnetic implants in configuration A (9)

- Group 2: Mice with magnetic implants in configuration B (9)

- Group 3: Mice without magnetic implants (9)

Group 4: Mice without magnetic implants (5).

2.9.2 2D mapping of magnetic flux

Two-dimensional magnetic flux maps of the *in vivo* implanted micromagnets for the A and B configurations in mice were obtained for groups 1 and 2 using a 10×10 mm^2 grid with 2 mm steps. For measurements, the mice were kept under anesthesia and placed on their backs onto a sliding platform table, placed on a precision XYZ manual linear positioning stage. Subsequently, a magnetic flux profile was recorded for both configurations along the main magnetic configuration axis (conventionally, the x-axis). These results were compared with preliminary 2D magnetic simulations of the two magnetic configurations obtained using the program FEMM 4.2 (Finite Element Method Magnetics).

2.9.3 Evaluation of Fe and sorafenib content in liver tissues

After 48 h of inserting the magnetic implants, groups 1, 2, and 3 received the intraperitoneal injection (100 µL) of Sorafenib/SPIONs/PEG-SLNs by using a 30G needle (230.0 mg/mL, 4.0 mg/mL, and 3.4 mg/mL for the formulation, sorafenib, and SPIONs, respectively). Group 4

received an intraperitoneal injection of phosphate buffer (10 mM, pH 7.4) and was used as a control. For each group, specimens were sacrificed after 3, 6, or 24 h after treatment by cervical dislocation, after anesthesia. All animal studies were conducted according to the standards approved by the Ethics Committee of the Italian Ministry of Health. The liver of each sacrificed mouse was cut into equal parts and rinsed with cold phosphate buffer on ice to remove any remaining luminal contents. A portion of the liver tissue was homogenized with ultrapure water using a tissue homogenizer at 4 °C. For Fe quantification, homogenates were digested with 3 mL of HNO_3 (67%)/H_2O_2 (30%), 1:1 (v/v), solution for 4 h at 60 °C in a stove. The Fe content was determined by performing ICP-MS using a Varian 820-MS ICP mass spectrometer. Sorafenib content in the tissue homogenates was evaluated by adding 6 mL of an acetonitrile:ethanol (2:1) mixture. After centrifugation at 12000 ×g for 20 min at 4 °C, supernatants were filtered through a polytetrafluoroethylene filter (0.2 μm), dried, and solubilized in methanol for HPLC analysis [55].

2.10. Statistical analysis

For *in vitro* and *in vivo* studies, statistical significance was calculated using a two-way analysis of variance (ANOVA) followed by Bonferroni post hoc tests (GraphPad Prism 5.0). Data were indicated with * $p<0.05$, ** $p<0.01$, and *** $p<0.001$.

3. Results and Discussion

PEG-stabilized SLNs, co-loaded with SPIONs and sorafenib, were prepared, characterized, and exploited as nanovectors, by performing *in vitro* and *in vivo* studies, for magnetic targeting of the therapeutic agent to the liver. The co-encapsulation of SPIONs and sorafenib in the PEG-SLNs (Sorafenib/SPIONs/PEG-SLNs) was expected to ensure the accumulation of sorafenib to the target

organ due to the magnetic field generated by the permanent micromagnets located in two different, purposely designed configurations, above the liver, after their under-skin implantation (Fig. 1).

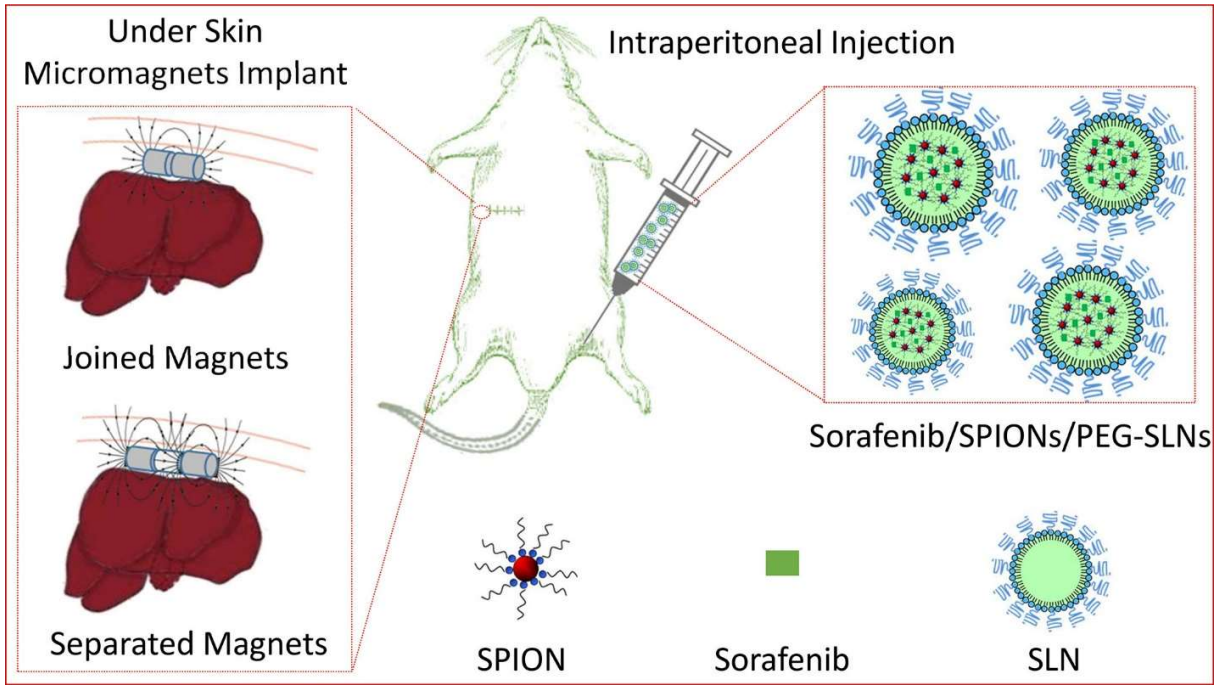

Fig. 1 Schematic representation of magnetic targeting to the liver based on the administration of Sorafenib/SPIONs/PEG-SLNs by intraperitoneal injection in living mice after the under-skin implantation, above the liver, of permanent micromagnets in two different configurations. Drawings not to scale.

3.1. Preparation of SLNs loaded with SPIONs and sorafenib

The preparation of Sorafenib/SPIONs/PEG-SLNs were prepared by exploiting a hot homogenization technique using CP as the lipid matrix and Tween 80 as the surface stabilizer [34]. First, empty and bare SLNs were prepared at different CP:Tween 80 weight ratios (0.3, 1.1, and 2.2) to identify the most suitable experimental conditions for the fabrication of SLNs characterized by high monodispersity and suitable colloidal stability in aqueous media (see Fig. S1 in the Supplementary Material). Based on the results obtained by performing DLS investigation and ζ-

potential measurements, the CP:Tween 80 ratio of 1.1 was found to be the most suitable to provide well-purified empty SLNs, with a monomodal size distribution, an average hydrodynamic diameter of 164 nm (polydispersity index [PDI] = 0.130 ± 0.010), and a ζ-potential of -15.9(±0.3) mV; therefore, the CP:Tween 80 ratio of 1.1 was later used for the preparation of SLNs based formulations. Stability tests were carried out by storing the SLNs in an aqueous solution after purification at three different temperatures (-22 °C, 4 °C, and 20 °C) for 10 days (see the Supplementary Material). DLS investigation (Fig. S2 in the Supplementary Material) revealed that 4 °C was the optimal storage temperature for the SLN aqueous solution. Upon definition of the most suitable experimental parameters for the SLN preparation and storage, Sorafenib/SPIONs/PEG-SLNs were prepared by keeping the sorafenib content constant and varying the starting SPION amount to modulate the magnetic cargo in the SLNs, a key factor influencing the magnetic targeting efficacy [49]. Generally, organic capped SPIONs were synthesized by exploring the hot decomposition of suitable organometallic precursors with coordinating solvents [47, 51].

The TEM micrograph shows SPIONs exhibiting a nearly spherical morphology (Fig. 2 (a)), characterized by a mean diameter of 6.1 (±0.6 nm, according to the statistical analysis).

The room temperature hysteresis loop of the “as synthesized” SPIONs indicated a completely anhysteretic magnetization, thus confirming their superparamagnetic character. The occurrence of maghemite (Fe_2O_3) [33] rather than magnetite (Fe_3O_4) [46] NPs was inferred by the saturation value (35.8 emu/g, at 55 kOe) (Fig. 2 (b)) [51].

SPIONs weight percentages of 1, 2, 2.5, and 3% (w/w with respect to CP) were tested to prepare Sorafenib/SPIONs/PEG-SLNs samples. The sorafenib amount was fixed at 0.5% (w/w with

respect to CP), and PEG-2-PE was added at a fixed concentration (4%, w/w with respect to CP) for the preparation of each sample (Fig. 2 (e)). PEG-2-PE was added to the lipid blend to improve the dispersion stability of SLNs in physiological environments via the steric stabilization effects of PEG moieties.

An increase in size was consistently observed with the increase in the SPION load (Fig. 2 (c) and (e)), namely, at size values of 135 (PDI = 0.157 ± 0.031), 142 (PDI = 0.153 ± 0.016), 149 (PDI = 0.204±0.022), and 164 nm (PDI = 0.165 ± 0.020) for SLNs with SPION at 1, 2, 2.5, and 3%, respectively.

The ζ-potential values recorded for the different samples (Fig. 2 (e)) generally agreed and were more negative than those obtained for SLNs without PEG owing to the phosphate moieties of the PEG-2-PE on the SLN surfaces.

SQUID measurements performed at room temperature on each prepared SPION-containing SLN sample demonstrated retention of the complete superparamagnetic character of the SPIONs after their encapsulation (Fig. 2 (d)), with the absolute value of magnetization increasing with the SPION content, as expected. The actual amount of SPIONs encapsulated in the SLNs was calculated for each sample by comparing the corresponding RT magnetic hysteresis cycle (Fig. 2 (d)) to that recorded for bare SPIONs (Fig. 2 (b)) [47]. The obtained data (Fig. 2 (e)) revealed that the actual SPIONs loads in the SLNs samples prepared from starting SPION amounts of 2.5 and 3% were closer to the corresponding theoretical values than the samples obtained using the lower tested SPION contents (1 and 2%). This evidence suggests that the hydrophobic SPION incorporation efficiency in the lipid matrix of the SLN cores was higher at their high starting contents (2.5 and 3%).

As the efficacy of magnetic targeting depends on the magnetic field intensity and SPION load, the sample featuring the highest actual load of SPIONs (1.65%) was selected for the following experiments to obtain a higher response of the system to the magnetic field. Indeed, such a value is comparable with that obtained by Al-Jamal et al., who prepared SPIONs containing polymeric/oil NPs at increasing amounts of SPIONs to enhance the magnetic forces generated from one small SPION, finding the optimal magnetic targeting condition at an actual SPION loading percentage of 1.76% [49].

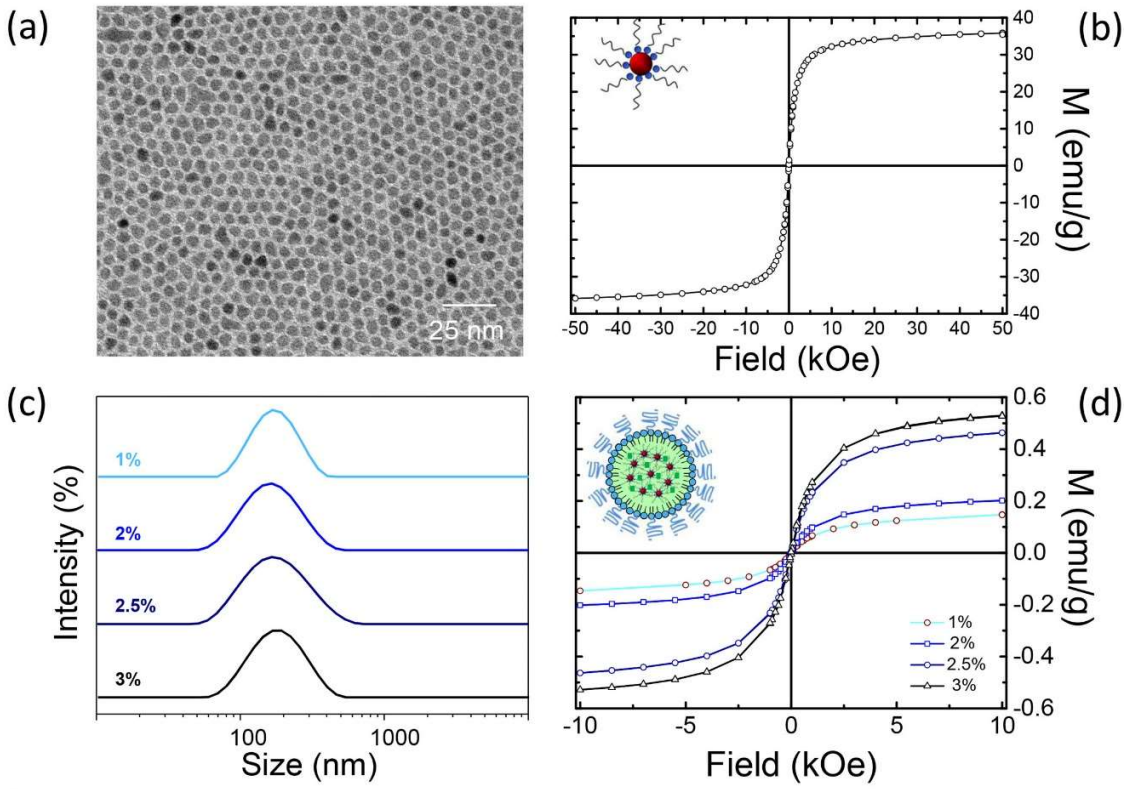

(e)

Sorafenib (%)	PEG-2-PE (%)	SPIONs (%)	D_H (nm)	PDI	ζ-Potential (mV)	M at 10 kOe (emu/g)	Actual SPIONs weight (%)	Theoretic SPIONs weight (%)
		100	-	-	-	32.20±0.01 (not at saturation)	-	-
0.5	4	1	135 ± 3	0.157± 0.031	-21.7 ± 0.8	0.15±0.01	0.47±0.06	0.62
		2	142 ± 2	0.153± 0.016	-21.2 ± 0.9	0.20±0.01	0.62±0.05	1.29
		2.5	149 ± 1	0.204± 0.022	-21.6 ± 0.3	0.46±0.01	1.43±0.01	1.46
		3	164 ± 1	0.165± 0.020	-21.0 ± 0.9	0.53±0.01	1.65±0.01	1.77

Fig. 2 TEM micrograph (a) and RT hysteresis cycle (b) of “as synthesized" SPIONs. Size distribution obtained using DLS (c) and RT hysteresis cycle of the Sorafenib/SPIONs/PEG-SLNs prepared from starting 0.5% sorafenib, 4% PEG-2-PE, and 1, 2, 2.5, or 3% of SPIONs (w/w with respect to the CP weight) (d). Table summarizing the characteristics of each Sorafenib/SPIONs/PEG-SLNs prepared sample, namely: average intensity hydrodynamic diameters (D_H), polydispersity index, and ζ-potential value; RT saturation magnetization (M) values of “as synthesized" SPIONs and Sorafenib/SPIONs/PEG-SLN samples; actual SPIONs content expressed as weight percentage in the different Sorafenib/SPIONs/PEG-SLN samples, as calculated from RT saturation magnetization (M) values; and theoretical SPION content calculated as the weight ratio percentage of the starting amount of SPIONs and amount of freeze-dried Sorafenib/SPIONs/PEG-SLNs, for each sample. All reported data are presented as mean values ± SD of three replicates (e).

As a subsequent step, Sorafenib/SPIONs/PEG-SLN samples with increasing drug contents of 0.5, 1, 2.5, and 5% (w/w with respect to CP) were prepared by keeping the CP:Tween 80 ratio, SPIONs, and PEG-2-PE weight percentages of 1.1, 3, and 4%, respectively.

Successful sorafenib loading inside the magnetic SLNs was assessed by performing HPLC quantification of the drug, and the effect of different drug feeding on encapsulation efficiency was investigated. Although the encapsulation load efficiency reached the maximum value (72.8%) for a drug feeding of 0.5% with an actual concentration of 1.14 mM, the highest actual loading (1.75%) and, consequently, the highest concentration (8.61 mM, 4 mg/mL) were achieved for the SLN formulation obtained at a starting sorafenib feed of 5% (Fig. 3). The obtained drug loading and encapsulation efficacy values were higher than those obtained in our previous study, in which PEG-modified phospholipid micelles were exploited as nanocarriers for the co-delivery of SPIONs and sorafenib [47]. Indeed, the encapsulation efficiency in micelles reached the maximum value (40%) when the feeding drug was 0.5 mg, with an actual loading of 150 μM, while the highest actual loading (235 μM) in the resulting nanoformulation was observed at a starting sorafenib feed of 1 mg. Furthermore, considering that the reported clinical studies indicate a therapeutic plasma concentration of sorafenib varying between 0.8 and 12.5%, it is worth noting that the formulation

obtained here, with an actual loading of 1.75%, designed to be intravenously administered, presents a clinically relevant concentration of sorafenib [56–60].

Based on the overall results, the Sorafenib/SPIONs/PEG-SLN formulation obtained from the starting 1.1, 3, 4, and 5% of CP:Tween 80 ratio, SPIONs, PEG-2-PE, and sorafenib weight percentages, respectively, was further characterized in terms of morphology, size, colloidal stability, PEG content, and MRI properties, as it was selected for use in the *in vitro* and *in vivo* experiments.

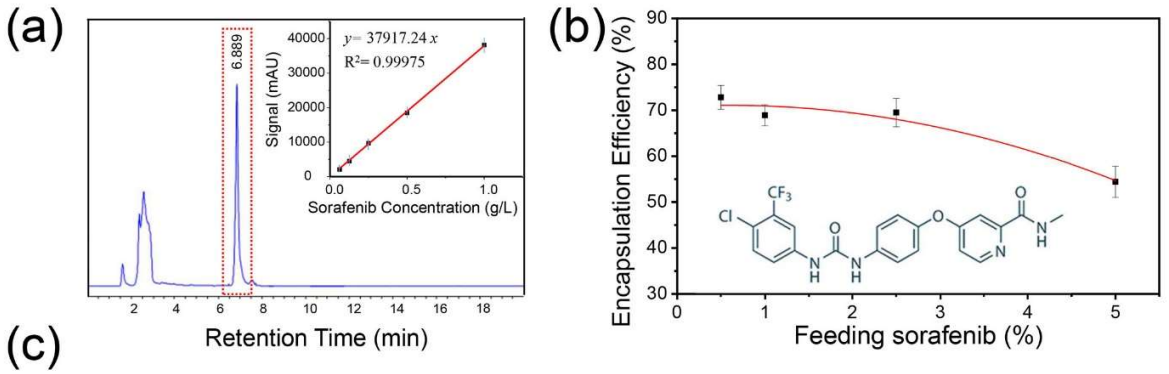

SPION (%)	PEG-2-PE (%)	Sorafenib (%)	EE (%)	DL (%)	Sorafenib Concentration (g/L)	Sorafenib Molarity (mM)
3	4	0.5	72.8 ± 2.6	0.21 ± 0.01	0.73 ± 0.03	1.14 ± 0.05
		1	68.9 ± 2.3	0.42 ± 0.02	1.38 ± 0.05	2.16 ± 0.04
		2.5	69.5 ± 3.1	1.10 ± 0.05	3.47 ± 0.04	5.45 ± 0.06
		5	54.4 ± 3.4	1.75 ± 0.05	5.44 ± 0.06	8.61 ± 0.05

Fig. 3 Representative HPLC chromatogram with UV detection at 250 nm of sorafenib after its extraction from Sorafenib/SPIONs/PEG-SLNs and calibration curve (a). Encapsulation efficiency percentage of sorafenib embedded in the different Sorafenib/SPIONs/PEG-SLNs as a function of the starting sorafenib feeding percentage (w/w with respect to CP), obtained using HPLC analysis (b). Summary table: encapsulation efficiency, drug loading, and concentration of sorafenib for each sample (c). All reported data are presented as mean values ± SD of three replicates.

3.2. Characterization of the formulation and assessment of MRI properties

The representative TEM micrograph, obtained by staining (Fig. 4 (a–a1)) the selected sample for 60 s, indicated the occurrence of spherically shaped SLNs with a size ranging from 50 to 210 nm, thus resulting in suitable agreement with the data obtained using DLS analysis and providing an average hydrodynamic diameter of 160 nm (PDI = 0.137 ± 0.01).

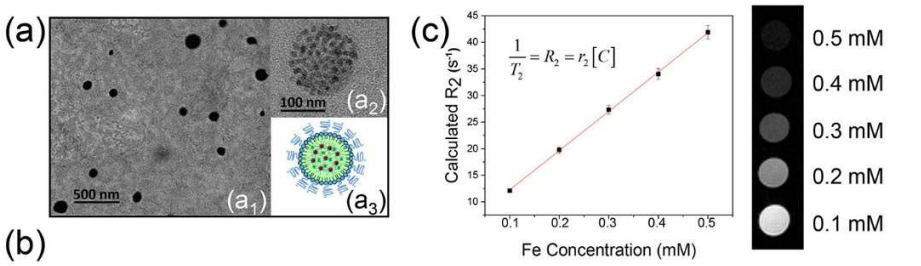

(b)

Sorafenib (%)	SPIONs (%)	PEG-2-PE (%)	Actual weight ratio PEG-2-PE/SLNs (%)	Incubation Time at 37°C (hours)	Sample Treatment	D_H Peak (nm)	Protein/SLNs (%)
5	3	0	0	0	Water	160 ± 1	-
					Serum	178 ± 4	13.5 ± 0.4
		4	0.42 ± 0.03	3	Water	168 ± 2	-
					Serum	173 ± 3	9.2 ± 0.3

Fig. 4 Representative TEM micrographs obtained at two different staining times, 60 (a_1) and 15 s (a_2) of Sorafenib/SPIONs/PEG-SLNs (sketched in the inset) prepared from starting CP:Tween 80 ratio, SPIONs, PEG-2-PE, and sorafenib weight percentages of 1.1, 3, 4, and 5%, respectively (a). Summary table: actual amount of PEG-2-PE in the formulation (Sorafenib/SPIONs/PEG-SLNs) obtained using molybdenum blue staining and expressed as PEG-2-PE/SLNs (w/w) ratio percentage; average intensity hydrodynamic diameter and amount of absorbed proteins expressed as protein/SLNs (w/w) ratio percentage for Sorafenib/SPIONs/PEG-SLNs and bare Sorafenib/SPIONs/SLNs, after incubation with human serum for 0 and 3 h at 37 °C (b). MR phantom test images with increasing Fe content and relative obtained graph with formula used to calculate the specific relaxivity index, r_2: 83.78 $mM^{-1}s^{-1}$, for Sorafenib/SPIONs/PEG-SLNs. All reported data are presented as mean values ± SD of three replicates (c).

Therefore, the average size of this PEG-functionalized NP sample (<200 nm), characterized by the highest load in both SPIONs and sorafenib, represents an adequate parameter, useful for taking advantage of the enhanced permeability and retention effect for penetration in tumors [49, 61, 62]. Interestingly, no significant change in the average hydrodynamic diameter was recorded over six

months for the samples stored at 4 °C. The representative TEM micrograph, recorded after 15 s sample staining (Fig. 4 (a-a2)), revealed a high SPION load in the formulation, as confirmed by the numerous SPIONs, visible as defined black spots well-confined within the spherical lipid matrix and clustered within a single SLN (Fig. 4 (a-a3)). In addition, a ζ-potential of -28.4(±0.4) mV was recorded, indicating the suitable colloidal stability of the sample in an aqueous medium.

Thin layer chromatography was used to confirm the presence of PEG-2-PE incorporated in the selected Sorafenib/SPIONs/PEG-SLNs and evaluate its actual content in the formulation (see details in the Supplementary Material). Molybdenum blue staining and video-densitometry allowed the detection and quantification of the content of the PEG-modified phospholipid, which was found to be 0.42(±0.03%) (Fig. 4b and Fig. S3 in the Supplementary Material) [63]. The PEG functionality at the SLN surface is expected to convey the improved SLN colloidal stability in physiological media, as well as stealth properties, limiting their arrest by macrophages, which eliminate exogenous objects in the body [64]. In this regard, the interaction of PEG-functionalized SLNs with the serum was investigated by incubating sorafenib/SPIONs/PEG-SLNs and human serum for 3 h at 37 °C. Bare sorafenib/SPIONs/SLNs at the same CP:Tween 80 ratio, SPION, and sorafenib weight percentages (1.1, 3, and 5%, respectively) without PEG-2-PE were also prepared and tested for comparison. SLNs with and without PEG-2-PE dispersed in water were used as corresponding controls for each sample (see Fig. S4 (a) and (c) in the Supplementary Material). After thorough purification, human serum protein absorption at the surfaces of the bare and PEGylated SLNs was investigated using DLS analysis and Bradford assay (Fig. 4 (b)) [52,65]. Interestingly, the monomodal size distributions, recorded using DLS analysis for the two samples, with and without PEG, treated with human serum for 3 h, proved their high colloidal stability in the biological medium (See Fig. S4 (b) and (d) in the Supplementary Material). However, only

bare Sorafenib/SPIONs/SLNs showed a statistically significant ($p<0.002$) increase of 18 nm in the average hydrodynamic diameter value after incubation with human serum for 3 h (Fig. S4 (a) and (b) in the Supplementary Material). By contrast, no statistically significant differences were found in the average hydrodynamic diameter of the PEGylated SLNs treated with human serum for 3 h, with only a slight shift, from 168 to 173 nm, observed in this case (Fig. S4 (c) and (d)). The Bradford assay allowed the calculation of a statistically significant ($p<0.001$) increase in the total amount of proteins (expressed as protein/SLNs (w/w) ratio percentage) adsorbed onto the bare SLNs (13.5%) when compared with the total protein content of the PEGylated SLNs (9.2%) (Fig. 4 (b)). Therefore, the ensemble of obtained DLS and Bradford assay results suggest that the presence of PEG molecules at the SLN surface was able to reduce, to some extent, the binding of macrophage-activating proteins, in contrast to the observation for the bare SLNs.

The MR phantom test carried out with Sorafenib/SPIONs/PEG-SLNs at five different Fe concentrations (0.5, 0.4, 0.3, 0.2, and 0.1 mM) revealed a calculated specific relaxivity of the sample of 83.78 $mM^{-1}s^{-1}$ (Fig. 4 (c)).

Therefore, considering the magnetic relaxivity properties arising from the encapsulation of SPIONs, Sorafenib/SPIONs/PEG-SLNs can also be envisioned as negative contrast agents for MRI, considering the features superior to those of other commercially available systems [33].

No significant release of sorafenib was detected by performing an *in vitro* drug release study on Sorafenib/SPIONs/PEG-SLNs using a Franz diffusion cell, thus confirming their stability in aqueous media. Therefore, drug release is expected to be induced by enzymatic degradation under *in vitro* cell culture or *in vivo* conditions [33, 34, 66, 67].

3.3. In vitro magnetic accumulation of SPIONs and sorafenib-loaded SLNs

Efficient retention of magnetic NPs at the desired target can be successfully achieved when the attractive magnetic forces exerted on them can overcome the opposing drag forces generated by the blood flow [68–70]. Therefore, an *in vitro* dynamic circuit simulating the hepatic blood flow in mice [71,72] was used to investigate the ability of the superparamagnetic SLNs to be captured in the accumulation system by using two very small joined NdFeB permanent magnets (north (N)-south (S) configuration) fixed to it by an adhesive tape. In Fig. 5 (a), an image of the dynamic circuit for the *in vitro* accumulation system is presented, and in Fig. 5 (b), the plot of the amount (as a percent of the initial content 98.5 mg/L) of captured Sorafenib/SPIONs/PEG-SLNs is reported.

A sudden increase in the capture extent of the magnetic SLNs in the presence of the permanent magnets was detected, following an asymptotic trend of up to 16.5%.

Therefore, the magnetic field resulting from two very small permanent magnets, joined side by side, is able to capture the magnetic SLNs at a starting SPION loading of 3%, thus allowing their application in under-skin implantation in *in vivo* experiments.

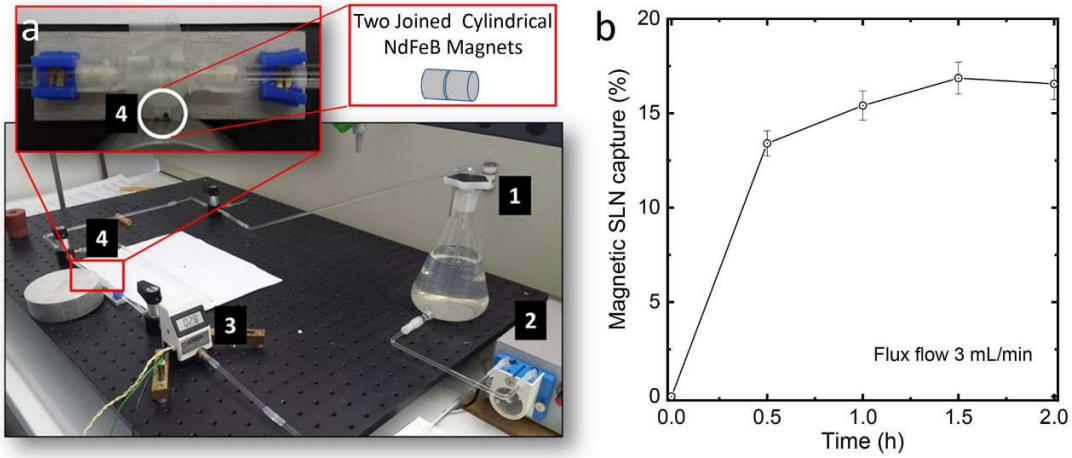

Fig. 5 Image of the *in vitro* dynamic circuit consisting of (1) an accumulation vessel, (2) a peristaltic pump (3 mL/min), (3) a digital flowmeter, (4) a magnetic accumulation system (a). Amount (as a percent of the initial content 98.5 mg/L) of captured Sorafenib/SPIONs/PEG-SLNs in the *in vitro* capillary flow model system. Data are reported as mean values ± SD of three replicates (b).

3.4. In vitro studies

A cell viability assay was performed on human liver cancer cells HepG-2. The effect of Sorafenib/SPIONs/PEG-SLNs on HepG-2 cell viability was determined using the MTT assay, with the data expressed as cell viability percentage and IC_{50} (μM) values (Fig. 6). In particular, the antiproliferative effect of Sorafenib/SPIONs/PEG-SLNs was compared with that of SPIONs/PEG-SLNs (as a function of embedded SPION concentration) (Fig. 6 (a)) or sorafenib alone (as a function of drug concentration) (Fig. 6 (b), (c)). The cell viability values obtained after 72 h Sorafenib/SPIONs/PEG-SLNs treatment were significantly lower than those observed for both SPIONs/PEG-SLNs, in the range of 1.4–14.5 μg/mL of SPIONs (Fig. 6 (a)), and for sorafenib alone in the range of 1–10 μM (Fig. 6 (b)).

Accordingly, the IC_{50} value at 72 h for the Sorafenib/SPIONs/PEG-SLNs (1.3(±0.1) μM of sorafenib) was lower than those of ones with sorafenib alone (2.3 (± 0.5) μM). However, for the highest tested concentrations, in terms of SPION and sorafenib encapsulated in SLNs, no differences in terms of cytotoxicity were detected. Therefore, for cell incubation times longer than 48 h, sorafenib was more effective when encapsulated in the SLNs rather than when freely available.

However, the cytotoxicity of Sorafenib/SPIONs/PEG-SLNs may not be ascribed only to the sorafenib load but also, in principle, to a partial, albeit lower contribution derived from the composition of the nanovectors. The IC_{50} values (Fig. 6 (c)) showed an increase in the cytotoxic activity of encapsulated sorafenib as a function of time; this trend was reasonably accounted for by a slower drug release, which would, however, turn into a longer-lasting effect over time.

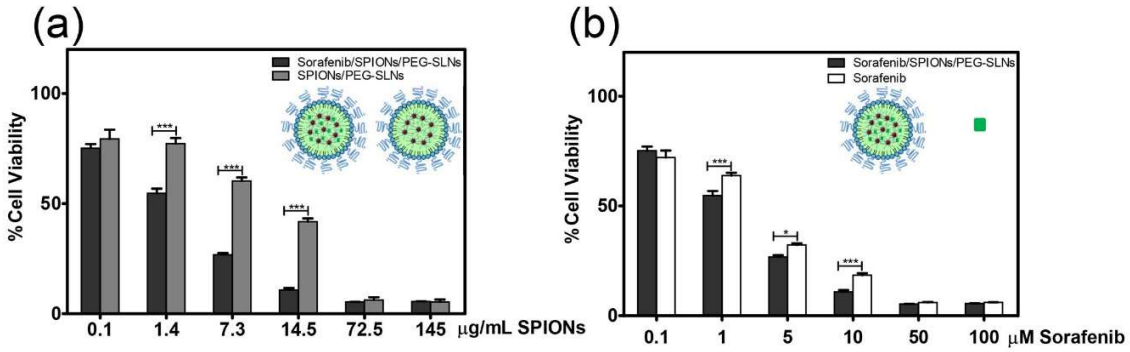

(c)

Sample	IC_{50} (μM)		
	24 h	48 h	72 h
Sorafenib	10.7 ± 2.1	2.8 ± 0.3	2.3 ± 0.5
Sorafenib/SPIONs/PEG-SLNs	16.6 ± 2.5	4.6 ± 1.1	1.3 ± 0.1

Fig. 6 Cell viability percentage of HepG-2 cells as a function of SPION concentrations (a) or sorafenib concentration (b) after 72 h of incubation. (c) IC_{50} values, in terms of sorafenib concentration, obtained using nonlinear regression in GraphPad Prism 5.0. Mean ± SD are reported, n = 3. Statistical significance was calculated using a two-way ANOVA followed by the Bonferroni post hoc tests (GraphPad Prism 5.0). Data are indicated with * $p<0.05$ and *** $p<0.001$.

3.5. Effect of magnetic targeting on cellular uptake

To assess the ability of the superparamagnetic SLNs to be internalized by HepG-2 cells, a concentration of SPIONs/PEG-SLNs (14.5 μg/mL in terms of SPIONs) was defined to not result

in cytotoxicity within the typical short times of an uptake experiment and was concurrently suited for analytical detection. The uptake experiment was conducted without applying a magnetic field and upon exposure to a ring magnet for 2 h or 4 h (Fig. 7). In particular, the application of an external magnetic field was performed by placing a ring magnet under the culture cell plate, as shown in Fig. 7 (a).

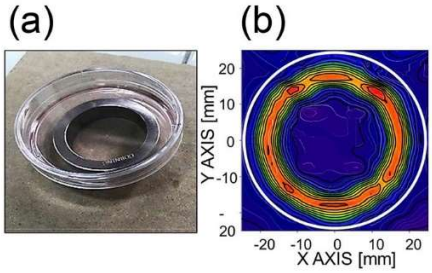

(c)

Fe Content in HepG-2 Cells (µg/L)		
Time Exposure (h)	Ring Geometry Magnet	No Magnet
2	1007.6 ± 10.2	232.1 ± 10.6
4	4152.3 ± 15.5	538.5 ± 9.5

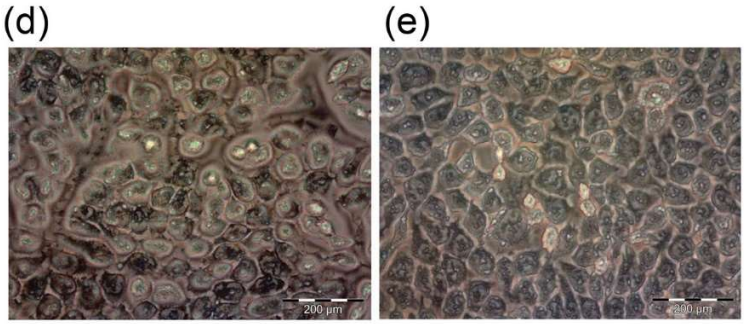

Fig. 7 Image of the HepG-2 liver cancer cells exposed to an external magnetic field generated using a ring magnet positioned under the cell culture plate (a). Graphical representation of the magnetic flux map generated using a ring magnet for the evaluation of SPIONs/PEG-SLNs uptake by HepG-2 liver cancer cells (b). Fe content (µg/L) determined using ICP-MS analysis in HepG-2 liver cancer cells after their incubation with SPIONs/PEG-SLNs for 2 h and 4 h in the presence or absence of magnetic field (c). Mean ± SD are reported, n = 3.; Prussian blue staining images by optical microscopy for HepG-2 cells after incubation with SPIONs/PEG-SLNs for 4 h in the absence (d); and presence (e) of the ring geometry magnet. Scale bar: 200 µm.

In this configuration, the ring magnet generated a magnetic flux, as shown in Fig. 7 (b). The presence of the magnetic field determined an increase in intracellular Fe content, measured by ICP-MS, after 2 h of cell incubation, that became even higher after 4 h ((1007.6 ± 10.2) and (4152.3

± 15.5) µg/L, respectively) than the corresponding value obtained without applying a magnetic field ((232.1 ± 10.6) and (538.5 ± 9.5) µg/L, respectively). In addition, the increase in intracellular uptake of SPIONs/PEG-SLNs upon application of an external magnetic field was qualitatively assessed through Prussian blue staining (Fig. 7 (d), (e)). Cells incubated with SPIONs/PEG-SLNs under exposure to the magnetic field revealed the presence of a number of blue spots (owing to the staining with Prussian Blue (Fig. 7 (e)) higher than that detected in the cells treated under the same experimental conditions but without applying a magnetic field (Fig. 7 (d)).

3.6. Recovery studies

The recovery experiment consisted of incubating HepG-2 cells with Sorafenib/SPIONs/PEG-SLNs for 4 h, and, as a reference, with sorafenib alone with or without a magnetic field. After 4 h, the cells were washed and allowed to grow for 24, 48, or 72 h in a fresh culture medium to obtain a sufficiently high intracellular uptake level, as revealed by *in vitro* uptake experiments. In Fig. 8, the histogram shows the cell viability percentages evaluated using the MTT test after the tested incubation times. A statistically significant time-dependent increase in the cytotoxic activity was observed when cells were treated with Sorafenib/SPIONs/PEG-SLNs rather than with free sorafenib in the presence of an external magnetic field (Fig. 8 (a), (b)). In the absence of a magnetic field, sorafenib encapsulated in the SLNs at the start time (T0) was less effective than sorafenib alone, while such a difference in cytotoxic activity disappeared at longer times, resulting in an antiproliferative effect at 72 h after the wash out, only slightly higher, and without statistical significance, than that obtained with free sorafenib (Fig. 8 (a), (b)).

As the magnetic field per se under the same conditions was not cytotoxic as previously reported [47], the results of the recovery study suggest that the application of an external magnetic field is

essential to promote higher nanoformulation accumulation inside the cells, which progressively releases sorafenib in a time-dependent manner, maintaining a longer-lasting intracellular drug concentration, higher than the free sorafenib.

(a)

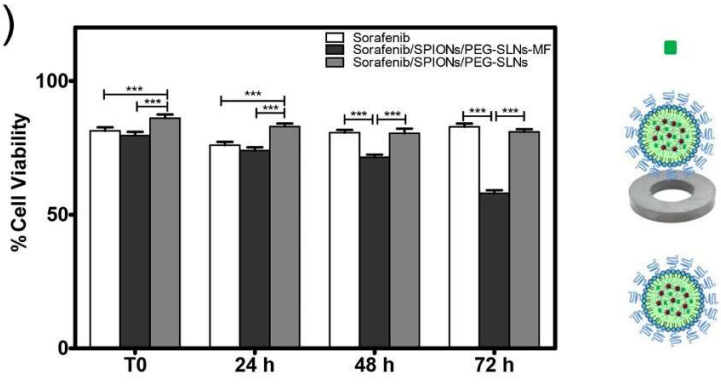

(b)

Sample	% Cell Viability			
	T0	24 h	48 h	72 h
Sorafenib	82 ± 1	76 ± 2	81 ± 1	83 ± 2
Sorafenib/SPIONs/PEG-SLNs-MF	79 ± 1	74 ± 1	71 ± 3	58 ± 3
Sorafenib/SPIONs/PEG-SLNs	86 ± 2	83 ± 3	80 ± 2	81 ± 1

Fig. 8 Cell viability of HepG-2 cells measured after incubation for 4 h with a different formulation, 10 µM sorafenib, exposed or unexposed to the magnetic field (MF) followed by wash out and culture in a fresh medium up to 24, 48, or 72 h (a). Summary table of the obtained data (b). Mean ± SD are reported, n = 3. Statistical significance was calculated using a two-way ANOVA followed by the Bonferroni post hoc tests (GraphPad Prism 5.0). Data are indicated with * $p<0.05$, ** $p<0.01$, and *** $p<0.001$.

3.7. Modeling of the different magnetic configurations and 2D simulation analysis

Preliminarily to the *in vivo* study, the two different magnet configurations were modelled, and 2D simulations of their magnetic field topographies were performed using FEMM software [73] to compute the *in vivo* magnetic forces acting on magnetic SLNs and optimize the *in vivo*

conditions for the magnetic targeting experiments in mice. For both configurations, two cylindrical (2×2×3 mm^3) NdFeB permanent magnets were selected for the simulation analysis. Configuration A recalled the same arrangement tested in the *in vitro* dynamic system, namely, two small, joined magnets attached to the accumulation system, as it was found to exert a magnetic field sufficiently intense to capture the SPIONs loaded SLNs. Configuration B was designed to form two magnets separated by a 5 mm thick Teflon spacer. For both magnet configurations, the N-S poles were oppositely positioned. In Fig. 9 (a) and (b), a map of the magnetic flux field density ((a) and (c)) for each designed magnet configuration is reported, where the mouse liver, represented as a closed blue line, is also drawn, at a distance of 2 mm (red line) from the magnets, to simulate the average *in vivo* distance between the under-skin magnetic implants and the mouse liver. In Fig. 9 (b) and (d), the plots of the variation of the magnetic induction B profile are depicted for the two configurations, along the x-axis and at a fixed distance (2 mm). For configuration B, a neat sinusoidal form of the profile of the magnetic flux was obtained (Fig. 9 (d)), whereas for configuration A, only a weak oscillation was detected (Fig. 9 (b)). These trends represent the magnetic gradient along the x-axis for the two configurations. Therefore, the magnetic gradient for configuration B is larger than that for configuration A, although the latter has a higher absolute value of the magnetic flux. The magnetic force acting on a magnetic NP with mass m_{NP} and magnetic susceptibility per mass unit χ_{NP} is defined by [47]:

$$F_M = \mu_0^2 m_{NP} \chi_{NP} \cdot H_z \cdot \mathrm{grad}(H) \qquad (1)$$

where, μ_0 is the vacuum permeability, H_z is the value of the magnetic field at a distance z from the magnet, and grad(H) is the gradient of the field, that is, the change in the field with the x and y directions at fixed z.

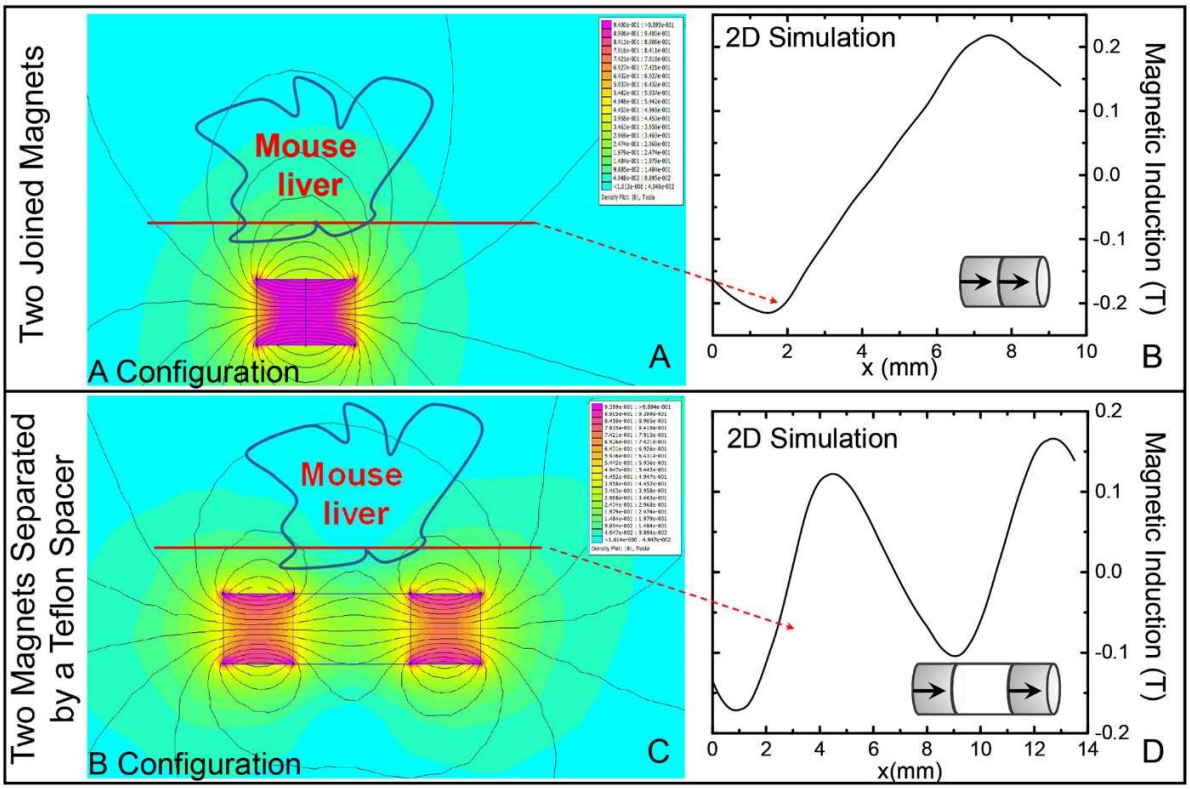

Fig. 9 2D simulations obtained using FEMM software: map of the magnetic flux field density ((a) and (c) and the corresponding magnetic induction profile, at a 2 mm fixed distance (indicated by the red line), along the x-axis ((b) and (d)) for the two different designed magnetic configurations, namely, two joined magnets ((a) and (b)) and two magnets separated by a Teflon spacer ((c) and (d)). The arrows in the sketches of the two magnetic configurations represent the magnetic field direction ((b) and (d)).

These simulations indicated that the product of the magnetic induction B multiplied by its gradient $\frac{dB}{dx}$, proportional to the magnetic attractive force, was larger for configuration B than for configuration A. This means that the attractive force acting on a magnetic NP was higher in the case of a configuration of two magnets separated by a non-magnetic spacer than in the configuration formed by two joined magnets.

3.8. In vivo studies

Following the previous results achieved by the simulation analysis, for *in vivo* experiments, the two different configurations of the NdFeB high-flux permanent micromagnets were implanted under the skin to assess their actual ability to capture and accumulate the magnetic SLNs in the liver tissues of the mice, thus finally defining the configuration resulting in the best magnetic performance. Therefore, the first configuration (A) was given by two magnets in close contact, and the second configuration (B) was of two magnets separated by a Teflon spacer with a thickness of 5 mm. For the *in vivo* study, wild-type mice C57BL/6J were investigated to assess the ability of the prepared nanoformulations to be magnetically guided to the target site (liver) and achieve organ-specific accumulation of SPIONs and sorafenib release. According to the *in vivo* administration of the prepared nanoformulations, the two under-skin permanent micromagnets were implanted above the livers of the mice by minimally invasive surgical intervention. The four groups of mice were tested. Two different configurations of micromagnets, A (joined magnets) and B (separated magnets), were implanted in mice of groups 1 and 2, respectively, as described in the Materials and methods section. Then, the magnetic induction was directly measured on sleeping mice under anesthesia and lying on their back on a precision XYZ manual linear positioning stage (Fig. 10 (a)). As shown in Fig. 10, the experimental *in vivo* magnetic induction measurements were performed along the main axis of the two magnetic configurations, A (joined magnets, Fig. 10 (b)) and B (separated magnets, Figure 10 (c)), respectively.

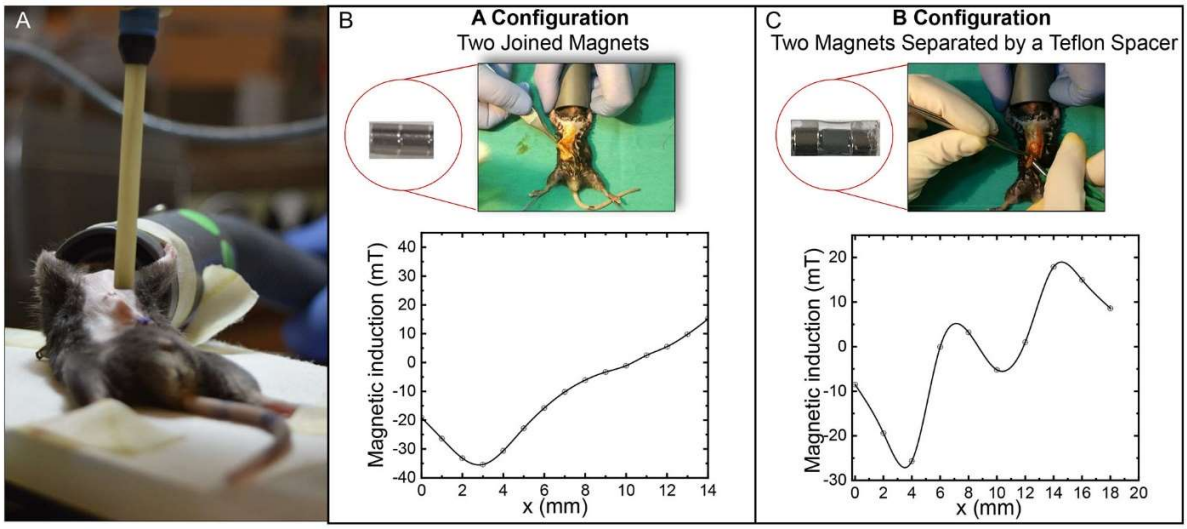

Fig. 10 Representative image of a sleeping mouse, placed on an XYZ 3-axis micropositioner stage, during the *in vivo* magnetic mapping of under-skin permanent magnets (a). *In vivo* magnetic induction profile, at a fixed distance, along the x-axis measured on a sleeping mouse for the two different magnetic configurations, namely, two joined magnets (b) and two magnets separated by a Teflon spacer (c). Images of experimental details can be seen in the (b) and (c) panels.

Two different profiles were detected for the two configurations, although the absolute values of the magnetic induction were comparable in the two cases. A comparison of the experimental (Figure 10 (b) and (c)) and of the 2D simulation (Figure 9 (b) and (d)) plots highlights a strong similarity in the trend of the curves, with the difference in the absolute value of the magnetic induction in the two cases due to the different actual distances of the magnetic sensor from the target, caused by a larger distance in the *in vivo* experiments (approximately 4 mm) than in the simulations (2 mm). Then, 48 h after the surgical intervention for the micromagnet implantation, Sorafenib/SPIONs/PEG-SLNs were administered by intraperitoneal injection to the mice of group 1 (implant with A configuration), 2 (implant with B configuration), and 3, which were not implanted, whereas group 4 (no implant and no treatment) was used as a control.

Intraperitoneal injection is a widely exploited administration route to test formulations in animals [74] and allows a direct approach to organs for drug transport through the mesenterical-portal vasculature, mesenterical-extraportal vasculature, extra-mesenterical vasculature, and lymph vessels [75]. After administering the SLN formulations, all mice from each group were sacrificed after 3, 6, and 24 h. The amounts of Fe and sorafenib in the liver samples of the sacrificed mice, processed as described in the Materials and methods section, were determined using ICP-MS and HPLC, respectively.

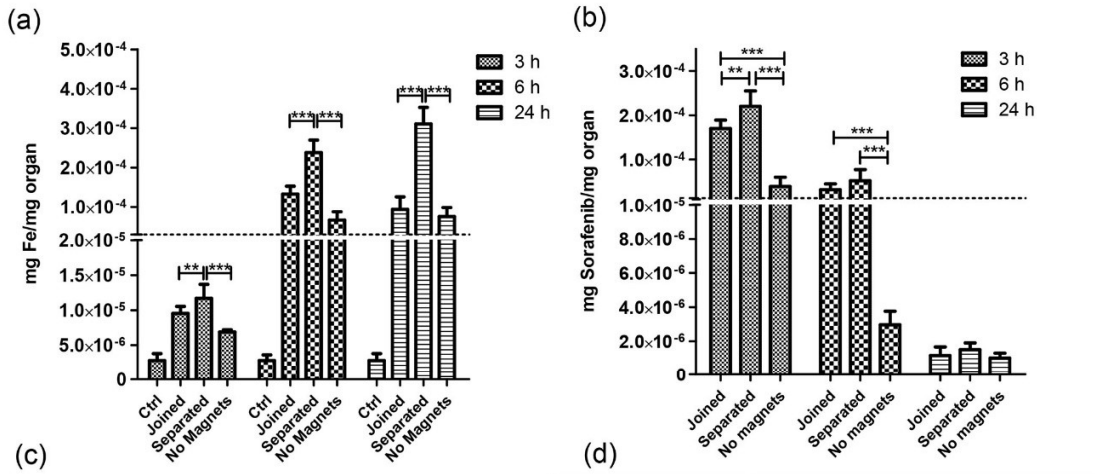

(c)

Sample	mg Fe/mg organ		
	3 h	6 h	24 h
Ctrl	(2.8±1.1) E-06	(2.8±1.1) E-06	(2.8±1.1) E-06
A Configuration (Joined magnets)	(9.5±1.0) E-06	(1.3±0.2) E-04	(9.4±3.2) E-05
B Configuration (Separated magnets)	(1.2±0.2) E-05	(2.4±0.3) E-04	(3.1±1.2) E-04
No Magnets	(6.9±0.3) E-06	(6.7±2.1) E-05	(7.6±2.3) E-05

(d)

Sample	mg Sorafenib/mg organ		
	3 h	6 h	24 h
A Configuration (Joined magnets)	(1.7±0.2) E-04	(3.2±1.3) E-05	(1.2±0.5) E-06
B Configuration (Separated magnets)	(2.2±0.4) E-04	(5.2±2.5) E-05	(1.5±0.4) E-06
No Magnets	(3.9±2.1) E-05	(2.9±0.8) E-06	(1.0±0.3) E-06

Fig. 11. Amount (mg Fe/mg organ) of Fe detected using ICP-MS analysis on homogenated murine liver samples ((a), (c)). Amount of sorafenib determined using HPLC analysis of processed murine liver samples ((b), (d)). Mean ± SD are reported, n = 9. Statistical significance was calculated using a two-way ANOVA followed by the Bonferroni post hoc tests (GraphPad Prism 5.0). **$p<0.01$ and *** $p<0.001$.

The ICP-MS and HPLC analysis results are shown in Fig. 11 (b) and (d) and Fig. 11 (a) and (c), respectively, as the weight of Fe or sorafenib per weight of the initially analyzed tissue. A significant increase in the Fe accumulation in the tissues was found in the livers of the group 1, 2, and 3 mice, treated with superparamagnetic SLNs when compared to that of the control group (4). Remarkably, the Fe amount was found to be significantly higher in the presence of the magnetic field, and the B configuration (separated magnets) was more efficient than the A configuration (joined magnets) in promoting a time-dependent Fe accumulation in the tissue, concurring with the prediction of the 2D simulation analysis. A significant increase in the amount of Fe in the livers of the mice of group 2 sacrificed at 6 h after the treatment and even higher Fe amount in those sacrificed after 24 h were recorded (Fig. 11 (a), (c)). The time-dependent monitoring of Fe accumulation in the tissues over 72 h was feasible because the local *in vivo* degradation of SPIONs was reported to occur very slowly (several months) [76]. Conversely, the amount of sorafenib in the tissues was much more abundant in the livers of mice sacrificed after 3 or 6 h from the treatment than in those sacrificed after 24 h for each treated group. Such time-dependent decrease could be accounted for by drug metabolism processes taking place once the drug is released into cells [77,78]. Sorafenib accumulation was positively affected by the internal magnetic field, particularly when the separated magnetic configuration was applied, resulting in an improved effectiveness of the treatment after 3 and 6 h.

The overall results obtained by the performing the *in vivo* study first proved that the magnetic targeting accomplished through the internal magnetic field generated using the two different magnetic configurations was effective in accumulating magnetic SLNs in the liver, as shown by the comparison with the results obtained from passive targeting experiments (with no magnets).

4. CONCLUSIONS

The preparation of PEG-modified SLNs co-loaded with SPIONs and sorafenib was carried out by thoroughly investigating the role of relevant experimental parameters, such as the surfactant/lipid ratio, SPION and sorafenib content, size, colloidal stability in physiological media, actual SPIONs and sorafenib load, magnetic behavior, and imaging properties as MRI contrast agents, of the resulting formulations. The SLN sample featuring the highest obtained SPION and drug loading, average hydrodynamic diameter smaller than 200 nm, stealth properties, and relevant MRI features as negative contrast agents was selected for the *in vitro* and *in vivo* investigations.

An *in vitro* study performed on HepG-2 liver cancer cells showed that the accumulation of the magnetic formulations inside the cells was enhanced in the presence of an external magnetic field. Furthermore, SLN delivery ensured a release inside the cells over 72 h more controlled and sustained than that obtained with free sorafenib.

It is worth noting that the obtained formulation is characterized by an actual loading of 1.75%, corresponding to a drug concentration of 4 mg/mL, designed to be intravenously administered; this presented a clinically relevant concentration of sorafenib when the therapeutic plasma concentration of sorafenib (0.8–12.5 μg/mL) - widely documented in literature - is considered [57–60, 79–82]. Indeed, generally, 100% of a drug administered intravenously is immediately delivered to the systemic circulation in its active form and thus is able to successfully reach the target sites, bypassing the strong reduction in absorption observed in oral administration [56,83]. Of course, the dosage of the proposed new formulation requires correct development through suitable clinical studies to properly evaluate the bioavailability of sorafenib after its reformulation and address the minimal dosage to be administered to the patients to receive maximum benefits, such as the rapid

relief of symptoms, reduced side effects, the enhanced therapeutic action of the drug, and prolonged protection.

The ability of the magnetic field generated by two very small magnets to hold back the SPION-loaded SLNs was demonstrated using an *in vitro* flow system simulating the liver blood flow. Two different A and B magnetic configurations, featuring joined and separated magnets, respectively, were designed and tested *in vivo* after under-skin implantation, above the mouse liver, accomplished by a minimally invasive surgical intervention. *In vivo* magnetic induction measurements were carried out for each magnetic configuration, and both the resulting experimental plots exhibited a trend similar to that predicted by 2D simulation analysis, indicating that the B configuration featured a higher magnetic field gradient. Indeed, the Fe quantification in the liver tissues using ICP-MS proved the effectiveness of magnetic targeting of the SPION-loaded SLNs to the liver, concurring with the results obtained by experimental measurements of magnetic induction and theoretical 2D simulations.

Interestingly, the findings corroborate our hypothesis, as the magnetic field topography was found to effectively affect the accumulation of SPION-loaded formulations in the mouse liver, demonstrating that the separated magnetic configuration (B) had the highest targeting efficacy. Our study offers an original perspective on the poorly investigated role of magnetic field topography in *in vivo* magnetic targeting efficacy [24, 49, 68]. Indeed, the magnetic field gradient generated by the B configuration has been demonstrated to promote SPION accumulation in the target organ higher than that obtained by the A configuration, highlighting that the magnetic field topography strongly affects the magnetic targeting performance. The proposed modeling of magnetic configuration using two separate magnets allows regulating the intensity of the magnetic field gradient, providing real advances in magnetic targeting to improve the penetration of

magnetic NPs in tissues, as suggested by Z. Zhou et al. based on results recently reported by Liu et al. [24, 25].

To our best knowledge, this study represents one of the very few reports on the application of purposely designed internal magnetic fields for magnetic targeting to the liver. Indeed, in most studies, magnetic targeting to the liver was commonly obtained by applying an external magnetic field [27–29]. J. Wang et al. exploited an internal fixed magnetic field by inserting a magnetic biliary stent wire into the subcutaneous heterotopic liver cancer tissue to magnetically accumulate magnetic NPs loaded with 5-fluorouracil to the liver for HCC treatment, thus demonstrating an enhanced curative effect compared with the traditional methods based on the application of external magnetic fields. In particular, ten stent wires (0.5 cm in length and 0.03 cm in diameter) were fully embedded into the tumor tissue by inserting them crosswise from different layers [31]. Here, we proposed the use of a minimally invasive skin magnetic implants that can be located above the liver, thus preventing damage to the peritoneum surrounding the organ and avoiding the actual risk of spreading cancer cells during surgical intervention.

A preclinical study suggested that the prepared MRI-traceable and superparamagnetic formulations, loaded with sorafenib, could offer enhanced therapeutic opportunities and improved survival of HCC patients in the future, enabling effective magnetic targeting to the liver upon their administration in the presence of an internal magnetic field.

In conclusion, while further optimization of specific issues, including the correct development of proper drug dosage of the new formulation and consideration of the anatomic constraints, is required before clinical translation, the proposed nanoformulation enables the use of a customized under-skin magnetic implants that can be surgically located above the liver and near cancerous

sites and then removed after suitable cycles of treatment, representing a minimally invasive and temporary strategy to perform an effective magnetic targeting to the liver without exposing patients to external magnetic devices for several hours, consequently reducing their burden.

Declaration of Competing Interest

The authors declare that they have no known competing financial interests or personal relationships that could have appeared to influence the work reported in this paper.

Acknowledgments

The authors acknowledge the Inter-University Consortium for Research on the Chemistry of Metal Ions in Biological Systems (C.I.R.C.M.S.B.) for their technical support.

Funding

This research was funded by the University of Bari "Aldo Moro" grant: Fondi di Ateneo and partially funded by Italian Regione Puglia, grant number: Tecnopolo per la Medicina di Precisione (CUP B84I1800054002).

Author Contributions

Investigation: *R. M. Iacobazzi, F. Vischio, I. Arduino, F. Canepa, E. Fanizza, A. Lopalco, M. Notarnicola, G. Bianco, M. P. Scavo, B. C. Lee*; **Conceptualization:** *N. Depalo, N. Denora;* **Data curation***: R. M. Iacobazzi, F. Vischio, N. Depalo, N. Denora;* **Formal Analysis:** *N. Depalo, N. Denora, F. Canepa, A. A. Lopedota, V. Laquintana, M. Notarnicola, M. L. Curri, A. Azzariti;* **Funding Acquisition***: N. Denora, A. Azzariti, M. L. Curri, G. Giannelli*; **Methodology:** *N. Depalo, N. Denora, F. Canepa, V. Laquintana, A. Lopalco, M. P. Scavo;* **Project Administration:** *N. Denora, N. Depalo;* **Supervision***: N. Denora, N. Depalo*; **Writing – original draft:** *N. Depalo,*

R. M. Iacobazzi, F. Vischio, F. Canepa, M. P. Scavo, N. Denora; **Writing – review & editing:** *M. Franco, A. Cutrignelli, M. L. Curri, R. M. Iacobazzi, F. Vischio, G. Giannelli, N. Depalo, N. Denora*

References

[1] B. Daniele, A.E. Brunetti, F. Fiore, E. Al, Linee guida Epatocarcinoma, Assoc. Ital. Di Oncol. Medica. (2018).

[2] A. Likhitsup, N. Razumilava, N.D. Parikh, Treatment for Advanced Hepatocellular Carcinoma: Current Standard and the Future, Clin. Liver Dis. 13 (2019) 13–19. https://doi.org/10.1002/cld.782.

[3] J.D. Yang, P. Hainaut, G.J. Gores, A. Amadou, A. Plymoth, L.R. Roberts, A global view of hepatocellular carcinoma: trends, risk, prevention and management, Nat. Rev. Gastroenterol. Hepatol. 16 (2019) 589–604. https://doi.org/10.1038/s41575-019-0186-y.

[4] H.B. El-Serag, Hepatocellular carcinoma, N. Engl. J. Med. 365 (2011) 1118–1127. https://doi.org/10.1056/NEJMra1001683.

[5] P. Wang, Z. Jiang, X. Liu, K. Yu, C. Wang, H. Li, L. Zhong, PI16 attenuates response to sorafenib and represents a predictive biomarker in hepatocellular carcinoma, Cancer Med. 9 (2020) 6972–6983. https://doi.org/10.1002/cam4.3331.

[6] Y. Li, Z.-H. Gao, X.-J. Qu, The Adverse Effects of Sorafenib in Patients with Advanced Cancers, Basic Clin. Pharmacol. Toxicol. 116 (2015) 216–221. https://doi.org/10.1111/bcpt.12365.

[7] A. Azzariti, S. Mancarella, L. Porcelli, A.E. Quatrale, A. Caligiuri, L. Lupo, F. Dituri, G.

Giannelli, Hepatic stellate cells induce hepatocellular carcinoma cell resistance to sorafenib through the laminin-332/α3 integrin axis recovery of focal adhesion kinase ubiquitination, Hepatology. 64 (2016) 2103–2117. https://doi.org/10.1002/hep.28835.

[8] B. Zhai, Mechanisms of resistance to sorafenib and the corresponding strategies in hepatocellular carcinoma, World J. Hepatol. 5 (2013) 345. https://doi.org/10.4254/wjh.v5.i7.345.

[9] L. Jain, S. Woo, E.R. Gardner, W.L. Dahut, E.C. Kohn, S. Kummar, D.R. Mould, G. Giaccone, R. Yarchoan, J. Venitz, W.D. Figg, Population pharmacokinetic analysis of sorafenib in patients with solid tumours, Br. J. Clin. Pharmacol. 72 (2011) 294–305. https://doi.org/10.1111/j.1365-2125.2011.03963.x.

[10] Y. Tsume, D.M. Mudie, P. Langguth, G.E. Amidon, G.L. Amidon, The Biopharmaceutics Classification System: Subclasses for *in vivo* predictive dissolution (IPD) methodology and IVIVC, Eur. J. Pharm. Sci. 57 (2014) 152–163. https://doi.org/10.1016/j.ejps.2014.01.009.

[11] C. Koch, M. Göller, E. Schott, O. Waidmann, M. op den Winkel, P. Paprottka, S. Zangos, T. Vogl, W.O. Bechstein, S. Zeuzem, F.T. Kolligs, J. Trojan, Combination of Sorafenib and Transarterial Chemoembolization in Selected Patients with Advanced-Stage Hepatocellular Carcinoma: A Retrospective Cohort Study at Three German Liver Centers, Cancers (Basel). 13 (2021) 2121. https://doi.org/10.3390/cancers13092121.

[12] Y. Zhao, W.J. Wang, S. Guan, H.L. Li, R.C. Xu, J.B. Wu, J.S. Liu, H.P. Li, W. Bai, Z.X. Yin, D.M. Fan, Z.L. Zhang, G.H. Han, Sorafenib combined with transarterial chemoembolization for the treatment of advanced hepatocellular carcinoma: a large-scale multicenter study of 222 patients, Ann. Oncol. 24 (2013) 1786–1792.

https://doi.org/10.1093/annonc/mdt072.

[13] J.-F.H. Geschwind, P.M. Gholam, A. Goldenberg, P. Mantry, R.C.G. Martin, B. Piperdi, E. Zigmont, J. Imperial, S. Babajanyan, P.K. Foreman, A. Cohn, Use of Transarterial Chemoembolization (TACE) and Sorafenib in Patients with Unresectable Hepatocellular Carcinoma: US Regional Analysis of the GIDEON Registry, Liver Cancer. 5 (2016) 37–46. https://doi.org/10.1159/000367757.

[14] T. Tamai, K. Kumagai, H. Sakae, H. Onishi, K. Tabu, E. Tabu, K. Muromachi, A. Saishoji, K. Oda, S. Mawatari, A. Moriuchi, K. Sakurai, A. Ido, Early sorafenib induction after transarterial chemoembolization for unresectable hepatocellular carcinoma: Can sorafenib after TACE improve loco-regional control?, Mol. Clin. Oncol. (2017). https://doi.org/10.3892/mco.2017.1434.

[15] J.-W. Park, Y.J. Kim, D.Y. Kim, S.-H. Bae, S.W. Paik, Y.-J. Lee, H.Y. Kim, H.C. Lee, S.Y. Han, J.Y. Cheong, O.S. Kwon, J.E. Yeon, B.H. Kim, J. Hwang, Sorafenib with or without concurrent transarterial chemoembolization in patients with advanced hepatocellular carcinoma: The phase III STAH trial, J. Hepatol. 70 (2019) 684–691. https://doi.org/10.1016/j.jhep.2018.11.029.

[16] S. Baghel, H. Cathcart, N.J. O'Reilly, Polymeric Amorphous Solid Dispersions: A Review of Amorphization, Crystallization, Stabilization, Solid-State Characterization, and Aqueous Solubilization of Biopharmaceutical Classification System Class II Drugs, J. Pharm. Sci. 105 (2016) 2527–2544. https://doi.org/10.1016/j.xphs.2015.10.008.

[17] N. Mishra, N.P. Yadav, V.K. Rai, P. Sinha, K.S. Yadav, S. Jain, S. Arora, Efficient Hepatic Delivery of Drugs: Novel Strategies and Their Significance, Biomed Res. Int. 2013 (2013)

1–20. https://doi.org/10.1155/2013/382184.

[18] M. Li, W. Zhang, B. Wang, Y. Gao, Z. Song, Q.C. Zheng, Ligand-based targeted therapy: A novel strategy for hepatocellular carcinoma, Int. J. Nanomedicine. 11 (2016) 5645–5669. https://doi.org/10.2147/IJN.S115727.

[19] M.P. Scavo, A. Cutrignelli, N. Depalo, E. Fanizza, V. Laquintana, G. Gasparini, G. Giannelli, N. Denora, Effectiveness of a Controlled 5-FU Delivery Based on FZD10 Antibody-Conjugated Liposomes in Colorectal Cancer *In vitro* Models, Pharmaceutics. 12 (2020) 650. https://doi.org/10.3390/pharmaceutics12070650.

[20] R.M. Iacobazzi, L. Porcelli, A.A. Lopedota, V. Laquintana, A. Lopalco, A. Cutrignelli, E. Altamura, R. Di Fonte, A. Azzariti, M. Franco, N. Denora, Targeting human liver cancer cells with lactobionic acid-G(4)-PAMAM-FITC sorafenib loaded dendrimers, Int. J. Pharm. 528 (2017) 485–497. https://doi.org/10.1016/j.ijpharm.2017.06.049.

[21] B. Shapiro, S. Kulkarni, A. Nacev, S. Muro, P.Y. Stepanov, I.N. Weinberg, Open challenges in magnetic drug targeting, Wiley Interdiscip. Rev. Nanomedicine Nanobiotechnology. 7 (2015) 446–457. https://doi.org/10.1002/wnan.1311.

[22] P.M. Price, W.E. Mahmoud, A.A. Al-Ghamdi, L.M. Bronstein, Magnetic Drug Delivery: Where the Field Is Going, Front. Chem. 6 (2018). https://doi.org/10.3389/fchem.2018.00619.

[23] M. Shamsi, A. Sedaghatkish, M. Dejam, M. Saghafian, M. Mohammadi, A. Sanati-Nezhad, Magnetically assisted intraperitoneal drug delivery for cancer chemotherapy, Drug Deliv. 25 (2018) 846–861. https://doi.org/10.1080/10717544.2018.1455764.

[24] J.F. Liu, Z. Lan, C. Ferrari, J.M. Stein, E. Higbee-Dempsey, L. Yan, A. Amirshaghaghi, Z. Cheng, D. Issadore, A. Tsourkas, Use of Oppositely Polarized External Magnets To Improve the Accumulation and Penetration of Magnetic Nanocarriers into Solid Tumors, ACS Nano. 14 (2020) 142–152. https://doi.org/10.1021/acsnano.9b05660.

[25] Z. Zhou, Z. Shen, X. Chen, Tale of Two Magnets: An Advanced Magnetic Targeting System, ACS Nano. 14 (2020) 7–11. https://doi.org/10.1021/acsnano.9b06842.

[26] H. Kempe, S.A. Kates, M. Kempe, Nanomedicine's promising therapy: magnetic drug targeting, Expert Rev. Med. Devices. 8 (2011) 291–294. https://doi.org/10.1586/erd.10.94.

[27] D. Shao, J. Li, X. Zheng, Y. Pan, Z. Wang, M. Zhang, Q.-X. Chen, W.-F. Dong, L. Chen, Janus "nano-bullets" for magnetic targeting liver cancer chemotherapy, Biomaterials. 100 (2016) 118–133. https://doi.org/10.1016/j.biomaterials.2016.05.030.

[28] A. Luciani, C. Wilhelm, P. Bruneval, P. Cunin, G. Autret, A. Rahmouni, O. Clément, F. Gazeau, Magnetic targeting of iron-oxide-labeled fluorescent hepatoma cells to the liver, Eur. Radiol. 19 (2009) 1087–1096. https://doi.org/10.1007/s00330-008-1262-9.

[29] Z. Lin, J. Ding, G. Sun, D. Li, S. He, X. Liang, X. Huang, J. Xie, Application of Paclitaxel-loaded EGFR Peptide-conjugated Magnetic Polymeric Liposomes for Liver Cancer Therapy, Curr. Med. Sci. 40 (2020) 145–154. https://doi.org/10.1007/s11596-020-2158-4.

[30] W.-J. Xue, Y. Feng, F. Wang, Y.-B. Guo, P. Li, L. Wang, Y.-F. Liu, Z.-W. Wang, Y.-M. Yang, Q.-S. Mao, Asialoglycoprotein receptor-magnetic dual targeting nanoparticles for delivery of RASSF1A to hepatocellular carcinoma, Sci. Rep. 6 (2016) 22149. https://doi.org/10.1038/srep22149.

[31] J. Wang, G. Du, J. Zheng, B. Xiao, H. Li, H. Cheng, S. Zou, Magnetic biliary stent targeting to treat hepatoma combining with magnetic nanoparticles, J. Wuhan Univ. Technol. Sci. Ed. 23 (2008) 312–315. https://doi.org/10.1007/s11595-007-3312-6.

[32] V. Mishra, K.K. Bansal, A. Verma, N. Yadav, S. Thakur, K. Sudhakar, J.M. Rosenholm, Solid lipid nanoparticles: Emerging colloidal nano drug delivery systems, Pharmaceutics. 10 (2018). https://doi.org/10.3390/pharmaceutics10040191.

[33] A. Grillone, E.R. Riva, A. Mondini, C. Forte, L. Calucci, C. Innocenti, C. de Julian Fernandez, V. Cappello, M. Gemmi, S. Moscato, F. Ronca, R. Sacco, V. Mattoli, G. Ciofani, Active Targeting of Sorafenib: Preparation, Characterization, and *In vitro* Testing of Drug-Loaded Magnetic Solid Lipid Nanoparticles, Adv. Healthc. Mater. 4 (2015) 1681–1690. https://doi.org/10.1002/adhm.201500235.

[34] I. Arduino, N. Depalo, F. Re, R. Dal Magro, A. Panniello, N. Margiotta, E. Fanizza, A. Lopalco, V. Laquintana, A. Cutrignelli, A.A. Lopedota, M. Franco, N. Denora, PEGylated solid lipid nanoparticles for brain delivery of lipophilic kiteplatin Pt(IV) prodrugs: An *in vitro* study, Int. J. Pharm. 583 (2020) 119351. https://doi.org/10.1016/j.ijpharm.2020.119351.

[35] F. Vischio, E. Fanizza, V. De Bellis, T. Sibillano, C. Ingrosso, C. Giannini, V. Laquintana, N. Denora, A. Agostiano, M. Striccoli, M.L. Curri, N. Depalo, Near-Infrared Absorbing Solid Lipid Nanoparticles Encapsulating Plasmonic Copper Sulfide Nanocrystals, J. Phys. Chem. C. 123 (2019) 23205–23213. https://doi.org/10.1021/acs.jpcc.9b05897.

[36] N. Larson, H. Ghandehari, “Polymeric Conjugates for Anti-cancer Drug Delivery,” Chem. Mater. (2010) 50–52.

[37] N. Kamaly, Z. Xiao, P.M. Valencia, A.F. Radovic-Moreno, O.C. Farokhzad, Targeted polymeric therapeutic nanoparticles: design, development and clinical translation, Chem. Soc. Rev. 41 (2012) 2971. https://doi.org/10.1039/c2cs15344k.

[38] H. Wang, S. Sun, Y. Zhang, J. Wang, S. Zhang, X. Yao, L. Chen, Z. Gao, B. Xie, Improved drug targeting to liver tumor by sorafenib-loaded folate-decorated bovine serum albumin nanoparticles, Drug Deliv. 26 (2019) 89–97. https://doi.org/10.1080/10717544.2018.1561766.

[39] R. Poojari, A. V Sawant, S. Kini, R. Srivastava, D. Panda, Antihepatoma activity of multifunctional polymeric nanoparticles via inhibition of microtubules and tyrosine kinases, Nanomedicine. 15 (2020) 381–396. https://doi.org/10.2217/nnm-2019-0349.

[40] Y. Li, J. Wei, Y. Wei, L. Cheng, B. Guo, F. Meng, F. Li, Z. Zhong, Apolipoprotein E Peptide-Guided Disulfide-Cross-Linked Micelles for Targeted Delivery of Sorafenib to Hepatocellular Carcinoma, Biomacromolecules. 21 (2020) 716–724. https://doi.org/10.1021/acs.biomac.9b01419.

[41] Y. Zan, Z. Dai, L. Liang, Y. Deng, L. Dong, Co-delivery of plantamajoside and sorafenib by a multi-functional nanoparticle to combat the drug resistance of hepatocellular carcinoma through reprograming the tumor hypoxic microenvironment, Drug Deliv. 26 (2019) 1080–1091. https://doi.org/10.1080/10717544.2019.1654040.

[42] Z. Wang, K. Zhao, Y. Zhang, X. Duan, Y. Zhao, Anti-GPC3 Antibody Tagged Cationic Switchable Lipid-Based Nanoparticles for the Co-Delivery of Anti-miRNA27a And Sorafenib in Liver Cancers, Pharm. Res. 36 (2019) 145. https://doi.org/10.1007/s11095-019-2669-5.

[43] S.S. Moni, M.F. Alam, M.M. Safhi, M.H. Sultan, H.A. Makeen, M.E. Elmobark, Development of formulation methods and physical characterization of injectable sodium selenite nanoparticles for the delivery of sorafenib tosylate, Curr. Pharm. Biotechnol. 21 (2019). https://doi.org/10.2174/1389201021666191230124041.

[44] G. Tom, S. Philip, R. Isaac, P.K. Praseetha, S.G. Jiji, V.V. Asha, Preparation of an efficient and safe polymeric-magnetic nanoparticle delivery system for sorafenib in hepatocellular carcinoma, Life Sci. 206 (2018) 10–21. https://doi.org/10.1016/j.lfs.2018.04.046.

[45] L. Zhang, Gong, Zhang, Ma, Zhang, Shen, Targeted therapy for human hepatic carcinoma cells using folate-functionalized polymeric micelles loaded with superparamagnetic iron oxide and sorafenib *in vitro*, Int. J. Nanomedicine. (2013) 1517. https://doi.org/10.2147/IJN.S43263.

[46] Y.-J. Li, M. Dong, F.-M. Kong, J.-P. Zhou, Folate-decorated anticancer drug and magnetic nanoparticles encapsulated polymeric carrier for liver cancer therapeutics, Int. J. Pharm. 489 (2015) 83–90. https://doi.org/10.1016/j.ijpharm.2015.04.028.

[47] N. Depalo, R.M. Iacobazzi, G. Valente, I. Arduino, S. Villa, F. Canepa, V. Laquintana, E. Fanizza, M. Striccoli, A. Cutrignelli, A. Lopedota, L. Porcelli, A. Azzariti, M. Franco, M.L. Curri, N. Denora, Sorafenib delivery nanoplatform based on superparamagnetic iron oxide nanoparticles magnetically targets hepatocellular carcinoma, Nano Res. 10 (2017). https://doi.org/10.1007/s12274-017-1444-3.

[48] J. Dulińska-Litewka, A. Łazarczyk, P. Hałubiec, O. Szafrański, K. Karnas, A. Karewicz, Superparamagnetic Iron Oxide Nanoparticles—Current and Prospective Medical Applications, Materials (Basel). 12 (2019) 617. https://doi.org/10.3390/ma12040617.

[49] K.T. Al-Jamal, J. Bai, J.T.-W. Wang, A. Protti, P. Southern, L. Bogart, H. Heidari, X. Li, A. Cakebread, D. Asker, W.T. Al-Jamal, A. Shah, S. Bals, J. Sosabowski, Q.A. Pankhurst, Magnetic Drug Targeting: Preclinical *in vivo* Studies, Mathematical Modeling, and Extrapolation to Humans, Nano Lett. 16 (2016) 5652–5660. https://doi.org/10.1021/acs.nanolett.6b02261.

[50] S. Mukherjee, L. Liang, O. Veiseh, Recent Advancements of Magnetic Nanomaterials in Cancer Therapy, Pharmaceutics. 12 (2020) 147. https://doi.org/10.3390/pharmaceutics12020147.

[51] G. Siciliano, M. Corricelli, R.M. Iacobazzi, F. Canepa, D. Comegna, E. Fanizza, A. Del Gatto, M. Saviano, V. Laquintana, R. Comparelli, G. Mascolo, S. Murgolo, M. Striccoli, A. Agostiano, N. Denora, L. Zaccaro, M.L. Curri, N. Depalo, Gold-Speckled SPION@SiO 2 Nanoparticles Decorated with Thiocarbohydrates for ASGPR1 Targeting: Towards HCC Dual Mode Imaging Potential Applications, Chem. – A Eur. J. 26 (2020) 11048–11059. https://doi.org/10.1002/chem.202002142.

[52] K.H. Bae, J.Y. Lee, S.H. Lee, T.G. Park, Y.S. Nam, Optically traceable solid lipid nanoparticles loaded with sirna and paclitaxel for synergistic chemotherapy with in situ imaging, Adv. Healthc. Mater. 2 (2013) 576–584. https://doi.org/10.1002/adhm.201200338.

[53] Guide for the Care and Use of Laboratory Animals, National Research Council (US) Committee for the Update of the Guide for the Care and Use of Laboratory Animals, 2011. https://www.ncbi.nlm.nih.gov/books/NBK54050/.

[54] L. Cicero, S. Fazzotta, V.D. Palumbo, G. Cassata, A.I. Lo Monte, Anesthesia protocols in

laboratory animals used for scientific purposes, Acta Biomed. 89 (2018) 337–342. https://doi.org/10.23750/abm.v89i3.5824.

[55] A. Parvinian, L.C. Casadaban, Z.Z. Hauck, R.B. van Breemen, R.C. Gaba, Pharmacokinetic study of conventional sorafenib chemoembolization in a rabbit VX2 liver tumor model, Diagnostic Interv. Radiol. 21 (2015) 235–240. https://doi.org/10.5152/dir.2014.14394.

[56] L. Gong, M.M. Giacomini, C. Giacomini, M.L. Maitland, R.B. Altman, T.E. Klein, PharmGKB summary, Pharmacogenet. Genomics. 27 (2017) 240–246. https://doi.org/10.1097/FPC.0000000000000279.

[57] M. Fukudo, T. Ito, T. Mizuno, K. Shinsako, E. Hatano, S. Uemoto, T. Kamba, T. Yamasaki, O. Ogawa, H. Seno, T. Chiba, K. Matsubara, Exposure–Toxicity Relationship of Sorafenib in Japanese Patients with Renal Cell Carcinoma and Hepatocellular Carcinoma, Clin. Pharmacokinet. 53 (2014) 185–196. https://doi.org/10.1007/s40262-013-0108-z.

[58] W. Ruanglertboon, M.J. Sorich, A. Rowland, A.M. Hopkins, Effect of early adverse events resulting in sorafenib dose adjustments on survival outcomes of advanced hepatocellular carcinoma patients, Int. J. Clin. Oncol. 25 (2020) 1672–1677. https://doi.org/10.1007/s10147-020-01698-7.

[59] T.A. Labeur, Q. Hofsink, R.B. Takkenberg, O.M. van Delden, R.A.A. Mathôt, R. Schinner, P. Malfertheiner, H. Amthauer, K. Schütte, B. Basu, C. Kuhl, J. Mayerle, J. Ricke, H.-J. Klümpen, The value of sorafenib trough levels in patients with advanced hepatocellular carcinoma – a substudy of the SORAMIC trial, Acta Oncol. (Madr). 59 (2020) 1028–1035. https://doi.org/10.1080/0284186X.2020.1759826.

[60] H. Mai, J. Huang, Y. Zhang, N. Qu, H. Qu, G. Mei, J. Liu, X. Xu, L. Chen, In-vivo relation between plasma concentration of sorafenib and its safety in Chinese patients with metastatic renal cell carcinoma: a single-center clinical study, Oncotarget. 8 (2017) 43458–43469. https://doi.org/10.18632/oncotarget.16465.

[61] C. Saraiva, C. Praça, R. Ferreira, T. Santos, L. Ferreira, L. Bernardino, Nanoparticle-mediated brain drug delivery: Overcoming blood-brain barrier to treat neurodegenerative diseases, J. Control. Release. 235 (2016) 34–47. https://doi.org/10.1016/j.jconrel.2016.05.044.

[62] S. Wilhelm, A.J. Tavares, Q. Dai, S. Ohta, J. Audet, H.F. Dvorak, W.C.W. Chan, Analysis of nanoparticle delivery to tumours, Nat. Rev. Mater. 1 (2016). https://doi.org/10.1038/natrevmats.2016.14.

[63] N. Depalo, L. Catucci, A. Mallardi, A. Corcelli, A. Agostiano, Enrichment of cardiolipin content throughout the purification procedure of photosystem II, Bioelectrochemistry. 63 (2004) 103–106. https://doi.org/10.1016/j.bioelechem.2003.09.031.

[64] Z. Ding, N. Luo, H. Yue, Y. Gao, G. Ma, W. Wei, *In vivo* immunological response of exposure to PEGylated graphene oxide via intraperitoneal injection, J. Mater. Chem. B. 8 (2020) 6845–6856. https://doi.org/10.1039/D0TB00499E.

[65] D. Pozzi, G. Caracciolo, L. Digiacomo, V. Colapicchioni, S. Palchetti, A.L. Capriotti, C. Cavaliere, R. Zenezini Chiozzi, A. Puglisi, A. Laganà, The biomolecular corona of nanoparticles in circulating biological media, Nanoscale. 7 (2015) 13958–13966. https://doi.org/10.1039/C5NR03701H.

[66] I. Arduino, R.M. Iacobazzi, C. Riganti, A.A. Lopedota, M.G. Perrone, A. Lopalco, A. Cutrignelli, M. Cantore, V. Laquintana, M. Franco, M. Contino, N. Denora, Induced expression of P-gp and BCRP transporters on brain endothelial cells using transferrin functionalized nanostructured lipid carriers: A first step of a potential strategy for the treatment of Alzheimer's disease, Int. J. Pharm. 591 (2020). https://doi.org/10.1016/j.ijpharm.2020.120011.

[67] I. Arduino, Z. Liu, A. Rahikkala, P. Figueiredo, A. Correia, A. Cutrignelli, N. Denora, H.A. Santos, Preparation of cetyl palmitate-based PEGylated solid lipid nanoparticles by microfluidic technique, Acta Biomater. 121 (2021) 566–578. https://doi.org/10.1016/j.actbio.2020.12.024.

[68] B. Chertok, A.E. David, V.C. Yang, Brain tumor targeting of magnetic nanoparticles for potential drug delivery: Effect of administration route and magnetic field topography, J. Control. Release. 155 (2011) 393–399. https://doi.org/10.1016/j.jconrel.2011.06.033.

[69] S. Jeong, J. Song, W. Lee, Y.M. Ryu, Y. Jung, S.-Y. Kim, K. Kim, S.C. Hong, S.J. Myung, S. Kim, Cancer-Microenvironment-Sensitive Activatable Quantum Dot Probe in the Second Near-Infrared Window, Nano Lett. 17 (2017) 1378–1386. https://doi.org/10.1021/acs.nanolett.6b04261.

[70] Q.A. Pankhurst, J. Connolly, S.K. Jones, J. Dobson, Applications of magnetic nanoparticles in biomedicine, J. Phys. D. Appl. Phys. 36 (2003). https://doi.org/10.1088/0022-3727/36/13/201.

[71] C. Xie, W. Wei, T. Zhang, O. Dirsch, U. Dahmen, Monitoring of systemic and hepatic hemodynamic parameters in mice, J. Vis. Exp. (2014). https://doi.org/10.3791/51955.

[72] W.T. Stott, M.D. Dryzga, J.C. Ramsey, Blood-flow distribution in the mouse, J. Appl. Toxicol. 3 (1983) 310–312. https://doi.org/10.1002/jat.2550030607.

[73] K.B. Baltzis, The FEMM package: A simple, fast, and accurate open source electromagnetic tool in science and engineering, J. Eng. Sci. Technol. Rev. 1 (2008) 83–89. https://doi.org/10.25103/jestr.011.18.

[74] J.M. Baek, S.C. Kwak, J.-Y. Kim, S.-J. Ahn, H.Y. Jun, K.-H. Yoon, M.S. Lee, J. Oh, Evaluation of a novel technique for intraperitoneal injections in mice, Lab Anim. (NY). 44 (2015) 440–444. https://doi.org/10.1038/laban.880.

[75] Intraperitoneal Drug Administration, in: Handb. Behav. Neurosci., 1994: pp. 46–58. https://doi.org/10.1016/B978-0-444-81871-3.50010-2.

[76] M. Reinert, Schlachter, Bregy, Lönnfors, Vajtai, Bernau, T. Weitzel, Mordasini, Slotboom, Herrmann, Bogni, Hofmann, M. Reinert, M. Frenz, Metabolic pathway and distribution of superparamagnetic iron oxide nanoparticles: *in vivo* study, Int. J. Nanomedicine. (2011) 1793. https://doi.org/10.2147/IJN.S23638.

[77] C. Tlemsani, O. Huillard, J. Arrondeau, P. Boudou-Rouquette, A. Cessot, B. Blanchet, A. Thomas-Schoemann, R. Coriat, J.-P. Durand, J. Giroux, J. Alexandre, F. Goldwasser, Effect of glucuronidation on transport and tissue accumulation of tyrosine kinase inhibitors: consequences for the clinical management of sorafenib and regorafenib, Expert Opin. Drug Metab. Toxicol. 11 (2015) 785–794. https://doi.org/10.1517/17425255.2015.1030392.

[78] X. Sheng, T. Huang, J. Qin, Q. Li, W. Wang, L. Deng, A. Dong, Preparation, pharmacokinetics, tissue distribution and antitumor effect of sorafenib-incorporating

nanoparticles *in vivo*, Oncol. Lett. (2017). https://doi.org/10.3892/ol.2017.6934.

[79] J.W. Clark, J.P. Eder, D. Ryan, C. Lathia, H.-J. Lenz, Safety and Pharmacokinetics of the Dual Action Raf Kinase and Vascular Endothelial Growth Factor Receptor Inhibitor, BAY 43-9006, in Patients with Advanced, Refractory Solid Tumors, Clin. Cancer Res. 11 (2005) 5472–5480. https://doi.org/10.1158/1078-0432.CCR-04-2658.

[80] A. Awada, A. Hendlisz, T. Gil, S. Bartholomeus, M. Mano, D. de Valeriola, D. Strumberg, E. Brendel, C.G. Haase, B. Schwartz, M. Piccart, Phase I safety and pharmacokinetics of BAY 43-9006 administered for 21 days on/7 days off in patients with advanced, refractory solid tumours, Br. J. Cancer. 92 (2005) 1855–1861. https://doi.org/10.1038/sj.bjc.6602584.

[81] M. Moore, H.W. Hirte, L. Siu, A. Oza, S.J. Hotte, O. Petrenciuc, F. Cihon, C. Lathia, B. Schwartz, Phase I study to determine the safety and pharmacokinetics of the novel Raf kinase and VEGFR inhibitor BAY 43-9006, administered for 28 days on/7 days off in patients with advanced, refractory solid tumors, Ann. Oncol. 16 (2005) 1688–1694. https://doi.org/10.1093/annonc/mdi310.

[82] D. Strumberg, J.W. Clark, A. Awada, M.J. Moore, H. Richly, A. Hendlisz, H.W. Hirte, J.P. Eder, H. Lenz, B. Schwartz, Safety, Pharmacokinetics, and Preliminary Antitumor Activity of Sorafenib: A Review of Four Phase I Trials in Patients with Advanced Refractory Solid Tumors, Oncologist. 12 (2007) 426–437. https://doi.org/10.1634/theoncologist.12-4-426.

[83] E.T. Hellriegel, T.D. Bjornsson, W.W. Hauck, Interpatient variability in bioavailability is related to the extent of absorption: Implications for bioavailability and bioequivalence studies, Clin. Pharmacol. Ther. 60 (1996) 601–607. https://doi.org/10.1016/S0009-9236(96)90208-8.